Electrophysiological Characterization of Subtype-Specific Modulation and Activation of Acid-Sensing Ion Channel and Acid-Evoked Signaling by Thyroid hormone Triiodothyronine

Von der Fakultät für Mathematik und Naturwissenschaften der RWTH Aachen University zur Erlangung des akademischen Grades eines Doktors der Naturwissenschaften genehmigte Dissertation

vorgelegt von

Lu Qin, M.Sc.

aus

Zhengzhou, China

Berichter: *Prof. Dr. Marc Spehr*

Prof. Dr. Stefan Gründer

Prof. Dr. Frank Müller

Tag der mündlichen Prüfung: *15.01.2026*

Eidesstattliche Erklärung

Lu Qin

erklärt hiermit, dass diese Dissertation und die darin dargelegten Inhalte die eigenen sind und selbstständig, als Ergebnis der eigenen originären Forschung, generiert wurden.

Hiermit erkläre ich an Eides statt

1. Diese Arbeit wurde vollständig oder größtenteils in der Phase als Doktorand dieser Fakultät und Universität angefertigt;
2. Sofern irgendein Bestandteil dieser Dissertation zuvor für einen akademischen Abschluss oder eine andere Qualifikation an dieser oder einer anderen Institution verwendet wurde, wurde dies klar angezeigt;
3. Wenn immer andere eigene- oder Veröffentlichungen Dritter herangezogen wurden, wurden diese klar benannt;
4. Wenn aus anderen eigenen- oder Veröffentlichungen Dritter zitiert wurde, wurde stets die Quelle hierfür angegeben. Diese Dissertation ist vollständig meine eigene Arbeit, mit der Ausnahme solcher Zitate;
5. Alle wesentlichen Quellen von Unterstützung wurden benannt;
6. Wenn immer ein Teil dieser Dissertation auf der Zusammenarbeit mit anderen basiert, wurde von mir klar gekennzeichnet, was von anderen und was von mir selbst erarbeitet wurde;
7. Kein Teil dieser Arbeit wurde vor deren Einreichung veröffentlicht.

Datum

Unterschrift

Inhaltsverzeichnis

Abbreviations 5

1. Introduction 9

1.1. Acid-sensing ion channel (ASICs) *9*

1.1.1. ASIC1 11

1.1.2. ASIC3 13

1.1.3. Pharmacology of ASICs 15

1.2. Thyroid hormones (TH) *17*

1.2.1. Synthesis and secretion of thyroid hormones 17

1.2.2. Regulation of Thyroid hormone (TH) homeostasis 20

1.2.3. Action of Thyroid hormone (TH) 21

1.3. Aim of the Thesis *22*

2. Material and Methods 23

2.1. Materials *23*

2.1.1. Cell culture media and supplements 24

2.1.2. Buffers and solutions for two electrode voltage clamp (TEVC) 24

2.1.3. Buffer and solutions for patch-clamp and Ca^{2+} imaging experiments. 25

2.1.4. Laboratory devices 29

2.1.5. Plasmid vectors 30

2.1.6. Software 31

2.2. Methods *32*

2.2.1. TEVC (Two electrode voltage clamp) 32

2.2.2. Cell culture 34

2.2.3. Patch clamp technique 35

2.2.4. Ratiometric Ca^{2+} Imaging 37

2.2.5. Data analysis 38

3. Results 39

3.1. The effect of thyroid hormone (TH) on the biophysical properties of rat ASIC1a ... 39

3.1.1. rat ASIC1a currents are potentiated by T2, T3 and T4 39

3.1.2. T3 rapidly binds to and unbinds from rat ASIC1a 41

3.1.3. T3 increases the efficacy of protons to activate rat ASIC1a 43

3.2. The effect of the thyroid hormone T3 on the biophysical properties of rat ASIC3 ... 45

3.2.1. T3 potentiates transient rat ASIC3 currents and induces sustained currents 45

3.2.2. T3 increases the proton sensitivity of rat ASIC3 47

3.2.3. T3 shifts activation and SSD curves of rat ASIC3, increasing the window current 49

3.3. Effect of T3 on human ASICs 51

3.3.1. The human thyroid cell line Nthy-ori-3-1 expresses functional ASICs, which are not potentiated by T3 51

3.3.2. T3 sensitivity of human ASIC1a, ASIC3, and ASIC1a/3 heteromers 53

3.3.3. T3 strongly activates human ASIC3 with micromolar apparent affinity 56

3.3.4. T3 elicits amiloride-sensitive Na^+ currents in cells expressing human ASIC3 58

3.4. T3 induced outward current in Nthy-ori-3-1 cell line 60

3.4.1. Which extracellular stimulus triggers the outward current in Nthy-ori-3-1 cells? 60

3.4.2. Which conductance underlies the outward current – ion selectivity? 62

3.4.3. What is the mechanism underlying the induction of the outward current? 64

3.4.4. Ca^{2+} Imaging of pH and T3 Effects in Thyroid Cells 67

4. Discussion 69

4.1. Mechanistic diversity of T3 effects on ASIC channels 70

4.1.1. Effects of T3 on rat ASICs 70

4.1.2. Effects of T3 on human ASICs 73

4.2. Response of Nthy-ori-3-1 cells to T3 and acidic pH 75

4.2.1. Effect of T3 on endogenous ASICs in Nthy-ori-3-1 cells 75

4.2.2. Outward current induced by T3 and extracellular acidification in Nthy-ori-3-1 cells 75

4.2.3. Potential Additional Ion Channels in Nthy-ori-3-1 Cells 77

4.3. Physiological relevance of the T3 effects discovered in this thesis 78

4.4. Outlook 80

Literature 82

Abbreviations

DEG	-	Degenerin
ENaC	-	Epithelial Sodium Channel
TMD	-	transmembrane domain
ECD	-	extracellular domain
CNS	-	central nervous system
PNS	-	peripheral nervous system
SSD	-	steady-state desensitization
DRG	-	dorsal root ganglia
TG	-	trigeminal ganglia
GMQ	-	2-guanidine-4-methylquinazoline
LPC	-	lysophosphatidylcholine
AA	-	arachidonic acid
TA	-	tannic acid
T3	-	triiodothyronine
rT3	-	reverse T3
T4	-	thyroxine
T2	-	diiodothyronine
Tg	-	thyroglobulin
NIS	-	sodium/iodide symporter
TPO	-	thyroid peroxidase
DUOX	-	dual oxidase enzymes
H2O2	-	hydrogen peroxide
MIT	-	monoiodotyrosine
DIT	-	diiodotyrosine
IYD	-	iodotyrosine deiodinase
MCT	-	monocarboxylate transporter
THBP	-	thyroid hormone-binding protein
TBG	-	thyroxine-binding globulin
TTR	-	transthyretin
ALB	-	albumin
HPT		hypothalamic–pituitary–thyroid

TRH	-	thyrotropin-releasing hormone
TSH	-	thyroid-stimulating hormone
TSHR	-	thyroid-stimulating hormone receptor
GPCR	-	G protein-coupled receptor
PKA	-	protein kinase A
cAMP	-	cyclic AMP
PIP2	-	phosphatidylinositol 4,5-bisphosphate
PLC	-	phospholipase C
TH	-	thyroid hormones
THR	-	thyroid hormone receptor
RXR	-	retinoid X receptor
TR	-	thyroid hormone receptor
TTX	-	tetrodotoxin
nAChR	-	nicotinic acetylcholine receptor
TAAR	-	trace amine-associated receptor
DMSO	-	dimethylsulfoxide
FBS	-	Fetal bovine serum
DMEM	-	Dulbecco's Modified Eagle Medium
TEVC	-	two-electrode voltage clamp
PEI	-	polyethylenimine
gA’	-	gramicidin A

Summary

In this thesis, it has been discovered that thyroid hormones, particularly T3, can activate or modulate acid-sensing ion channels (ASICs) in a subtype-specific manner. For rat ASICs (rASICs), T3 enhanced the amplitude of rASIC1a and rASIC3 currents, but with different mechanisms. For rASIC1a, T3 increased proton efficacy without altering proton sensitivity. This was supported by the observation that T3 potentiated rASIC1a currents both at pH 6.5 (near its pH_{50}) and at pH 6.0 (when the channel is fully activated). In contrast, T3 increased the proton affinity of rASIC3 without affecting its proton efficacy. This was evident from a leftward shift in both the activation and steady-state desensitization (SSD) curves. Since the activation curve shifted more strongly than the SSD curve, the overlap between them, corresponding to the window current, was enlarged.

For human ASICs (hASICs), T3 exhibited subtype-specific effects as well. Similar to rASICs, T3 also potentiated hASIC1a transient currents. However, in the case of homomeric hASIC3, T3 directly activated the channel at neutral or even alkaline pH, inducing a sustained inward current. This T3-induced current was sensitive to amiloride, a classical ASIC blocker, and had a positive reversal potential, suggesting it was carried primarily by Na^+ ions. Interestingly, T3 did not modulate or activate the heteromeric hASIC1a/3 channel. These findings were observed with recombinant ASICs expressed either in *Xenopus* oocytes or in human embryonic kidney (HEK) cells. Endogenous ASIC currents in the human thyroid epithelial cell line Nthy-ori-3-1 were not potentiated by T3, suggesting that heteromeric ASIC1/3 channels predominate in these cells.

In addition to ASIC-related effects, an outward current was observed in Nthy-ori 3-1 cells when T3 was applied at low extracellular pH. This current was mediated by Ca^{2+}-activated potassium channels, which were activated in response to increased intracellular Ca^{2+} concentrations. Since both the outward current and Ca^{2+} signaling were abolished by YM-254890, a broad-spectrum inhibitor of G protein-coupled receptor (GPCR) pathways, it is likely that this response was initiated via activation of an unidentified GPCR.

Zusammenfassung

In dieser Doktorarbeit wurde gezeigt, dass Schilddrüsenhormons, insbesondere T3, „Acid-Sensing Ion Channels“ (ASICs) auf subtypspezifische Weise aktiviert oder moduliert. Bei ASICs der Ratte (rASICs) verstärkte T3 die Stromamplitude von rASIC1a und rASIC3, jedoch über unterschiedliche Mechanismen. Für rASIC1a erhöhte T3 die Protoneneffizienz, ohne die Protonenaffinität zu verändern. Dies wurde durch die Beobachtung gestützt, dass T3 die rASIC1a-Ströme bei pH 6,5 (nahe dem pH_{50}) und bei pH 6,0 (wenn die Kanäle vollständig aktiviert sind) potenzierte. Im Gegensatz dazu erhöhte T3 bei rASIC3 die Protonenaffinität, ohne die Protoneffizienz zu beeinflussen. Dies zeigte sich in einer Linksverschiebung sowohl der Aktivierungs- als auch der Gleichgewichts-Desensitivierungskurve (SSD). Da die Aktivierungskurve stärker verschoben wurde als die SSD-Kurve, vergrößerte sich die Überlappung der beiden Kurven, was dem sogenannten „window current“ entspricht.

Auch bei ASICs des Menschen (hASICs) zeigte T3 subtypspezifische Effekte. Ähnlich wie bei rASICs potenzierte T3 die hASIC1a-Ströme. Im Fall des homomeren hASIC3 jedoch aktivierte T3 den Kanal bei neutralem oder sogar alkalischem pH direkt und löste einen anhaltenden Einwärtsstrom aus. Dieser durch T3 induzierte Strom war empfindlich für Amilorid, einem klassischen ASIC-Inhibitor, und wies ein positives Umkehrpotential auf, was darauf hindeutet, dass er hauptsächlich durch Na^+-Ionen getragen wurde. Interessanterweise wurde der heteromere hASIC1/3-Kanal durch T3 weder moduliert noch aktiviert. Diese Ergebnisse wurden mit rekombinanten ASICs erworben, die entweder in *Xenopus* Oozyten oder in der humanen HEK-Zelllinie exprimiert worden waren. Endogene ASIC-Ströme in der menschlichen thyreoidalen Epithelzelllinie Nthy-ori 3-1 wurden nicht durch T3 potenziert, was darauf hindeutet, dass in diesen Zellen hauptsächlich heteromere ASIC1/3-Kanäle exprimiert werden.

Neben den ASIC-assoziierten Effekten wurde in Nthy-ori 3-1-Zellen auch ein Auswärtsstrom beobachtet, wenn T3 bei saurem extrazellulären pH appliziert wurde. Dieser Strom wurde durch kalziumaktivierte Kaliumkanäle vermittelt, die durch einen Anstieg der intrazellulären Kalziumkonzentration aktiviert wurden. Da sowohl der Auswärtsstrom als auch das Kalziumsignal durch YM-254890 – einen Breitbandinhibitor G-Protein-gekoppelter Rezeptoren (GPCRs) – unterdrückt wurden, nehmen wir an, dass diese Antwort durch Aktivierung eines bislang unbekannten GPCR ausgelöst wird.

1. Introduction

1.1. Acid-sensing ion channel (ASICs)

Acid-Sensing Ion Channels (ASICs) are proton-sensitive cation channels that are mainly permeable to Na^+. ASICs belong to the Degenerin/Epithelial Sodium Channel (DEG/ENaC) superfamily. Mammals express six ASIC subunits: ASIC1a, ASIC1b, ASIC2a, ASIC2b, ASIC3, and ASIC4, which are encoded by four genes (*Asic1–Asic4*). These subunits assemble into homo- or heteromeric ion channels with distinct pH sensitivities and physiological functions [1, 2].

The first high-resolution crystal structure of a chicken ASIC (cASIC1) was solved in 2007 (Fig. 1A), providing critical insights into their architecture. ASICs consist of short intracellular N- and C-termini, two transmembrane domains (TMDs), and a large extracellular domain (ECD), which accounts for approximately 70% of the total protein. Structurally, a single ASIC subunit resembles a clenched arm, where the TMDs represent the forearm, and the ECD forms a fist-like structure, which is composed of multiple domains, including the palm, finger, thumb, β-ball, and knuckle domains [3-5].

Upon rapid extracellular acidification, ASICs typically exhibit a transient inward current, characterized by three primary conformational states: resting, open, and desensitized (Fig. 1B) [6]. When the extracellular proton concentration increases, ASICs open via proton binding to the acidic pocket, a key region located between the finger and thumb domains. Structural studies with cASIC1 have identified two critical carboxyl-carboxylate interactions (Asp238 - Asp350 and Glu239 - Asp346, respectively) that play a pivotal role in ASIC activation [3]. Upon activation, ASICs transition from the resting to the open state, allowing the influx of Na^+. Cation permeation through the ion pore is regulated by the GAS motif in TM2, which forms the narrowest constriction in the open-state channel pore and acts as the selectivity filter [7]. Following activation, ASICs rapidly (within < 1 sec or a few seconds) enter a desensitized state, during which the upper part of the ECD remains protonated and static, while the lower ECD and TMD adopt a resting-like conformation and the pore is closed again. The β11-12 linker in the lower ECD, particularly residues L414 and N415, has been shown to be essential for this transition. When the extracellular pH returns to neutral values, the acidic pocket releases protons, and the channel transitions back to the resting state, ready for reactivation upon subsequent acidification [8].

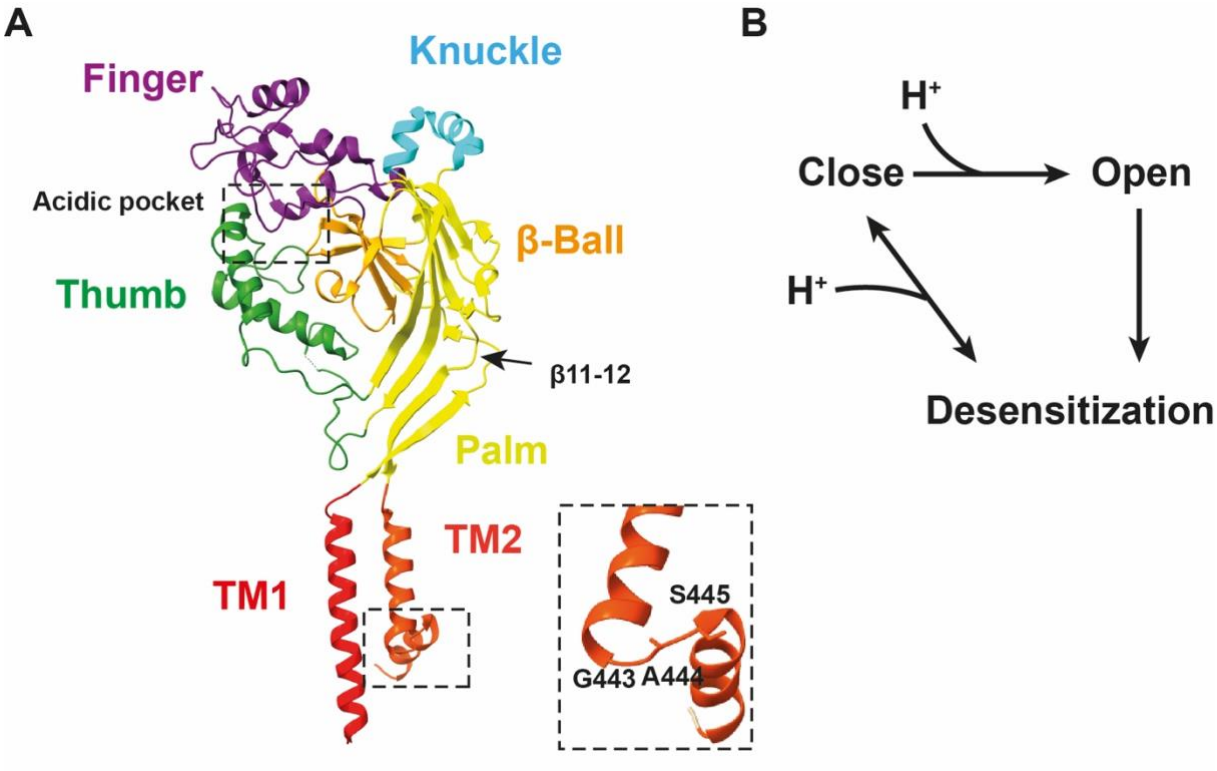

Figure 1. Structure and conformation state of ASIC1a. (A) X-ray structure of cASIC1a (PDB: 4NTX), with domain specification based on the 'clenched fist' model proposed by Jasti et al. (2007). GAS motif magnified. (B) Simplified kinetic scheme illustrating the three conformational states of ASICs.

1.1.1. ASIC1

ASIC1 is encoded by the *Asic1* gene and is widely expressed in the nervous system. ASIC1 exists in two isoforms, ASIC1a and ASIC1b, which exhibit distinct distribution patterns and functional roles [9].

ASIC1a is primarily expressed in the central nervous system (CNS), including the cortex, hippocampus, amygdala, hypothalamus, and pituitary [10]. It plays a critical role in neuronal excitability, synaptic plasticity, and sensory perception and has been implicated in learning, fear conditioning, memory processing, and regulation of the daily temperature rhythm [10-14]. In contrast, ASIC1b is predominantly expressed in the peripheral nervous system (PNS), particularly in the dorsal root ganglia (DRG) and trigeminal ganglia (TG) [15, 16]. ASIC1b is primarily involved in pain sensation and mechanosensation [17-19]. ASIC1b is a splice variant of ASIC1a, differing in the N-terminal cytoplasmic domain–where ASIC1b contains an extended N-terminus (88 residues vs. 43 in ASIC1a)–, the first TMD and the proximal third of the ECD, while the distal ECD, the second TMD and the intracellular C-terminus of both isoforms are identical [9].

ASIC1a and ASIC1b share similar biophysical characteristics, mediating transient inward currents. Proton activation of these channels occurs in a concentration-dependent manner, with the current amplitude increasing with increasing acidification until saturation at around pH 6.0 for rat ASIC1a (rASIC1a) and pH 5.0 for rASIC1b [20]. The pH_{50} of activation represents the pH at which 50 % of the channels are activated; ASIC1b has a lower pH sensitivity than ASIC1a, with a pH_{50} of 5.84 - 6.03 versus 6.50 - 6.56 for ASIC1a [20-23]. In addition to activation, steady-state desensitization (SSD) is an essential biophysical property of ASICs. Under physiological conditions, the extracellular pH is buffered between pH 7.35 and 7.45, keeping most ASIC channels in the resting state, available for activation. SSD occurs when the extracellular pH slightly drops to a range (pH ~7.3–6.9) that is insufficient for full activation but sufficient to induce desensitization, rendering ASICs unresponsive to further acidification. The pH_{50} of SSD, indicating the pH at which 50 % of ASIC channels are desensitized at steady-state, is 7.19 - 7.30 for ASIC1a and 6.95 - 7.0 for ASIC1b [21, 24, 25], respectively.

Human ASIC1a (hASIC1a) and rASIC1a share a high sequence identity (98.1%; [26]) and exhibit comparable biophysical properties. The pH_{50} of activation for hASIC1a is 6.35 - 6.46, while the pH_{50} of SSD is 6.91 - 7.1, closely matching the values of rASIC1a [27-29]. These similarities suggest conserved functional properties across species, making rodent models relevant for studying ASIC1a physiology and pharmacology.

ASIC1 can assemble as a homomeric channel or as a heteromeric complex with other ASIC subunits, leading to diverse pH sensitivities, biophysical properties, and functional roles. In the CNS, ASIC1a commonly forms heteromers with ASIC2a (ASIC1a/2a) and ASIC2b (ASIC1a/2b) [30], which are highly expressed in neuronal circuits implicated in synaptic plasticity and learning [11]. In the PNS, ASIC1b preferentially assembles with ASIC2a (ASIC1b/2a) or ASIC3 (ASIC1b/3), where it plays a role in nociception and mechanosensation [17，31，32].

1.1.2. ASIC3

ASIC3 is encoded by the *Asic3* gene and, in rodents, is primarily expressed in the PNS, particularly in sensory neurons of the DRG and TG [33, 34]. In addition to its predominant expression in sensory neurons, ASIC3 is also found in lung epithelial cells [35], Smooth muscle [36], skeletal tissues [37], and testis, where it was first cloned [38, 39]. Functionally, ASIC3 is involved in respiratory regulation and the perception of chronic inflammatory and ischemic pain, making it a key player in nociception and acid-induced signaling [18, 40].

Compared to ASIC1, ASIC3 exhibits lower protein sequence identity between rat and human isoforms (83.68%) and demonstrates species-dependent differences in both functional properties and expression patterns [26]. While no splice variants have been reported for rat ASIC3 (rASIC3), human ASIC3 (hASIC3) has three splice variants (hASIC3a, hASIC3b, hASIC3c), which differ in their N-terminal sequences [41]. These species-specific differences contribute to variations in pH sensitivity, desensitization kinetics, and other unique functional characteristics between rat and human ASIC3.

Similar to rASIC1a, proton activation induces a transient inward Na^+ current in rASIC3, which is followed by rapid desensitization. However, rASIC3 desensitizes more quickly than rASIC1a, with a time constant (τ) of around 0.35 ± 0.04 s, while rASIC1a desensitizes with t = 3.5 ± 0.39 [42]. rASIC3 is highly sensitive to protons, with an activation pH_{50} of 6.7 and a pH_{50} of SSD of 7.1 [42].

An important feature of ASIC3 is its ability to generate two types of acid-induced sustained currents: 1. Sustained currents that occur at strong acidification (< pH 5.0) and follow the transient current, typically with smaller amplitude. 2. Window currents that occur under mildly acidic conditions (pH 7.2–6.8) and arise due to the overlap of SSD and activation curves [43]. In this overlapping pH range, rASIC3 is partially activated without fully desensitizing, leading to a persistent inward current of small amplitude. The window current allows rASIC3 to sense moderate acidosis, making it crucial for detecting inflammatory pain and ischemia-induced acidification [43]. This sustained low-level activation allows ASIC3 to respond to prolonged pH fluctuations in chronic inflammatory states, muscle fatigue, and ischemic tissue damage [40, 42, 43].

Compared with rASIC3, hASIC3 exhibits lower proton sensitivity, with an activation pH_{50} around pH 6.0 [41, 44]. In addition to its response to acidic conditions, hASIC3 is unique in its ability to detect alkaline pH. This dual pH response is attributed to a specific arginine residue (R68/R83) in the extracellular loop, which is essential for alkaline pH sensing. This property distinguishes hASIC3 from its rodent counterpart, suggesting potential species-specific physiological roles for hASIC3 in sensory signaling under both acidic and alkaline conditions [41].

1.1.3. Pharmacology of ASICs

To date, various endogenous and exogenous ligands have been identified that can inhibit, modulate, or activate ASICs. Among these, amiloride is one of the most well-characterized non-selective pore blockers of the DEG/ENaC superfamily, which includes ENaC, ASIC, BASIC, pickpocket (PPK), NeNaC, and HyNaC [45-49]. Beyond this family, it also inhibits other ion channels and transporters, such as T-type Ca^{2+} channels (Ca_v3) and Na^+/H^+ exchangers (NHEs) [50，51]. In ASICs, amiloride acts by blocking the channel pore, thereby inhibiting the proton-induced transient current, with an IC_{50} of 10 μM for ASIC1a and ~20 μM for ASIC3 [1，52]. On the other hand, amiloride exhibits a dual modulatory effect on ASIC3. At low concentrations (e.g., 100 μM), it not only blocks the transient current evoked by acidic pH but also potentiates the sustained "window current" under near-neutral pH conditions (7.3–6.8). At higher concentrations, however, this window current is also inhibited, indicating a concentration-dependent bidirectional regulation [43，52]. In contrast, the second type of sustained current, which occurs after the transient current during strong acidification (pH < 5), remain controversial. Some studies have shown a potentiation effect [53], whereas others have observed inhibition or no significant change [54-56].

Mechanistically, this potentiation effect is associated with a non-proton ligand-sensing domain located in the palm domain of ASIC3, involving residues E79 and E423. This glutamate-rich region is proposed to interact with the alkaline functional groups of amiloride, thereby causing an alkaline shift in the activation and to a lesser extent the SSD curve, increasing the window current. The net effect is an increased probability of ASIC3 channel opening under mildly acidic to neutral conditions [52].

A similar mechanism has been reported for other basic ligands, such as 2-guanidine-4-methylquinazoline (GMQ) and the RFamide peptide RPRFa, both of which bind to the non-proton ligand-sensing domain and shift both activation and SSD curves, inducing a sustained current at physiological pH [57，58].

In addition to synthetic and peptide modulators, lipid-derived molecules also regulate ASIC3 activity. Notably, lysophosphatidylcholine (LPC) and arachidonic acid (AA) have been shown to activate both rASIC3 and hASIC3 at physiological pH [59]. Multiscale molecular dynamics simulations have revealed potential binding sites within the TMD, particularly involving residues R65 and R68 in hASIC3 [60].

Moreover, ASICs are also sensitive to indirect modulation by amphiphilic compounds. For instance, tannic acid (TA) has been shown to alter membrane properties, resulting in inhibition of ASIC activity through non-specific lipid bilayer effects rather than direct channel interaction [61]. These findings illustrate that ASIC function is not only regulated by proton binding but also highly sensitive to some small molecules depending on their chemical structure, charge, and membrane interaction.

1.2. Thyroid hormones (TH)

Thyroid hormones are essential regulators of numerous physiological processes, including metabolism, growth, development, and thermoregulation. These hormones are synthesized and secreted by the thyroid gland, a butterfly-shaped endocrine organ located in the anterior neck. The two primary thyroid hormones are thyroxine (T4) and triiodothyronine (T3), which contain four and three iodine atoms, respectively. While T4 is predominantly produced by thyroid follicular epithelial cells and generally considered a prohormone, T3 represents the biologically active form, which can be synthesized directly by the thyroid or converted peripherally from T4 through deiodination [62].

Structurally, thyroid hormones possess two benzene rings, and the iodine atoms on the outer ring significantly influence the pKa of the phenolic hydroxyl group (OH) (Fig. 2). The pKa of this group is approximately 6.8 for T4 and 8.4 for T3, meaning that at pH 6.8 and pH 8.4, around 50 % of the phenolic OH groups of T4 and T3, respectively, are in their protonated form [63，64]. This chemical characteristic may influence their ionization state, membrane permeability, and potential interactions with proteins, such as ASICs.

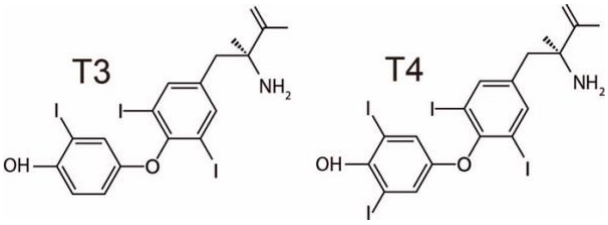

Fig. 2. Structure of thyroid hormones T3 and T4.

1.2.1. Synthesis and secretion of thyroid hormones

The thyroid gland is composed primarily of thyroid epithelial cells, also known as thyrocytes, which are the main functional cell type. These cells are organized into spherical structures called follicles, each surrounding a central lumen filled with a dense, protein-rich material. The apical membrane of thyrocytes faces the follicular lumen, while the basal membrane interfaces with the surrounding capillary network (Fig. 3).

Thyrocytes are responsible for the synthesis and secretion of thyroglobulin (Tg), a large glycoprotein precursor of thyroid hormones T3 and T4. Tg is synthesized in the endoplasmic

reticulum, processed through the trans-Golgi network, and transported via secretory vesicles to the apical membrane, where it is exocytosed into the follicular lumen [65]. Within the lumen, Tg accumulates at very high concentrations, reaching up to 800 mg/ml [66]. Most of the thyroglobulin in the follicular lumen is insoluble, forming multilayered, quasi-crystalline thyroid globules, which serve as the storage form of covalently cross-linked thyroglobulin. These insoluble globules are surrounded by a layer of highly concentrated soluble thyroglobulin of varying thickness. This entire structure is collectively referred to as the thyroid colloid [66].

The biosynthesis of thyroid hormones requires iodide uptake from the bloodstream into the thyrocytes. This process occurs through the sodium/iodide symporter (NIS) located on the basolateral membrane. Iodide is then transported into the follicular lumen across the apical membrane via the anion exchanger pendrin. In the colloid, iodide (I^-) is oxidized to reactive iodine (I^0) by thyroid peroxidase (TPO) in a reaction that depends on hydrogen peroxide (H_2O_2) generated by dual oxidase enzymes (DUOX1/2) [62，66].

The activated iodine is covalently attached to specific tyrosine residues on thyroglobulin, forming monoiodotyrosine (MIT) and diiodotyrosine (DIT). Subsequent coupling reactions, also catalyzed by TPO, lead to the formation of thyroxine (T4, corresponding to DIT + DIT) and triiodothyronine (T3, MIT + DIT), which remain attached to the Tg molecule and are stored in the colloid [66].

When needed, Tg containing T3 and T4 is taken up by endocytosis into follicular cells and transported to lysosomes, where it is cleaved by lysosomal enzymes into free T3 and T4, whereas uncoupled MIT and DIT are deiodinated by iodotyrosine deiodinase (IYD), allowing the released iodide to be recycled for further hormone synthesis. The free T3 and T4 are then exported across the basolateral membrane into the circulation via the monocarboxylate transporter 8 (MCT8) and monocarboxylate transporter 10 (MCT10) [67，68]. Approximately 90 % of secreted hormone is T4 and around 10 % is T3, reflecting their relative abundances in the circulation [66].

Once released into the bloodstream, the vast majority of thyroid hormones are bound to thyroid hormone-binding proteins (THBPs) for transport to target tissues. The primary THBPs include thyroxine-binding globulin (TBG), transthyretin (TTR), and albumin (ALB). More than 99 % of circulating thyroid hormones are protein-bound, leaving only a small fraction in the free (unbound) form, which is considered biologically active [69]. Specifically, < 0.03 % of plasma

T4 (approximately 15 pM) and around 0.3 % of plasma T3 (approximately 5 pM) circulate as free hormones [63，69，70].

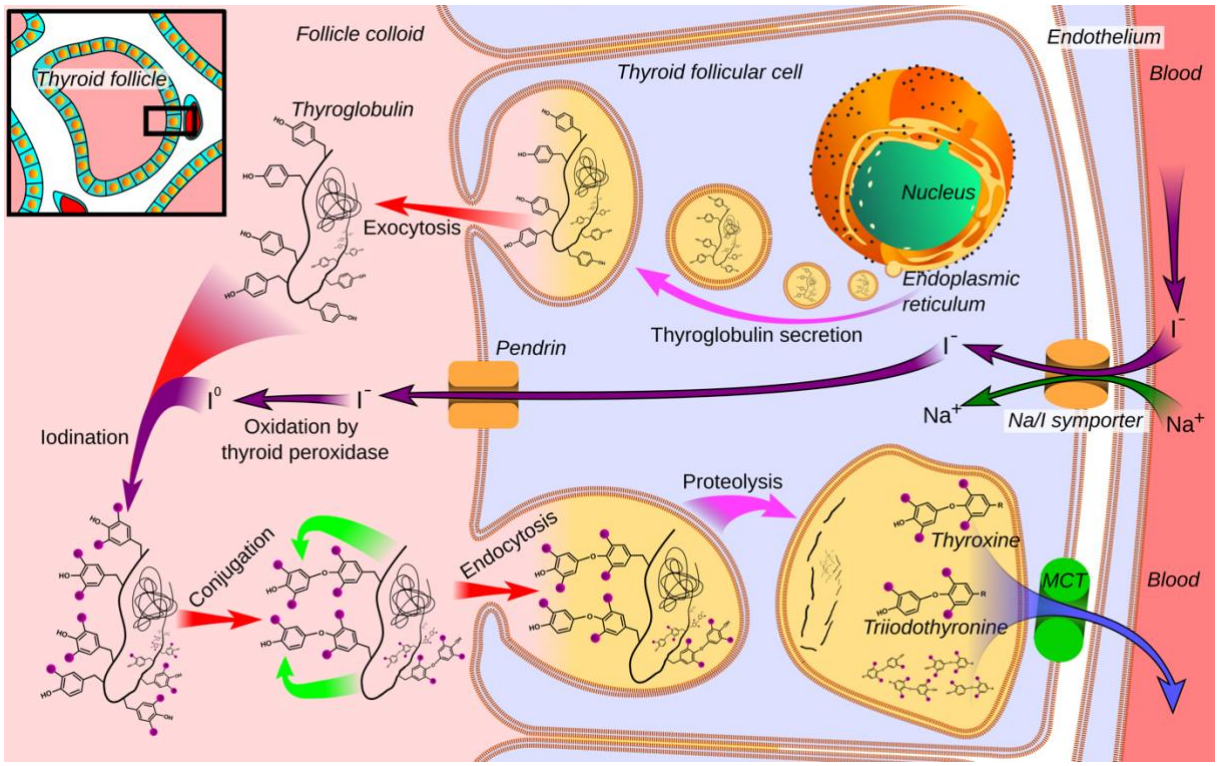

Fig. 3. Synthesis of thyroid hormones. For details, see the text. From Boron et al. 2003 **[71].**

1.2.2. Regulation of Thyroid hormone (TH) homeostasis

Thyroid hormone homeostasis is primarily regulated by the hypothalamic–pituitary–thyroid (HPT) axis. A decrease in circulating TH levels stimulates the hypothalamus to secrete thyrotropin-releasing hormone (TRH), which in turn promotes the release of thyroid-stimulating hormone (TSH) from the anterior pituitary. TSH then binds to the TSH receptor (TSHR) on the surface of thyroid epithelial cells (thyrocytes), a G protein-coupled receptor (GPCR) that activates multiple intracellular signaling cascades to enhance TH synthesis and secretion [62]. TSHR signals through both the Gs and Gq pathways [72].

At low TSH concentrations (e.g., 0.3 mU/mL), TSHR primarily activates the Gs pathway, leading to an increase in cyclic AMP (cAMP) levels and subsequent activation of protein kinase A (PKA) [72]. The cAMP/PKA pathway plays a central role in regulating several key processes in thyroid hormone biosynthesis. It upregulates the expression and activity of the NIS and also promotes NIS translocation from intracellular vesicles to the basolateral membrane, thereby enhancing iodide uptake from the plasma [73-76]. In addition, pendrin, the apical iodide transporter, is stimulated to translocate to the apical membrane, facilitating iodide efflux into the follicular lumen [77]. Furthermore, TSH stimulates the expression of Tg and TPO via the cAMP/PKA pathway, providing the necessary substrates for TH synthesis [78]. The release of thyroglobulin into the follicular lumen is also enhanced through this pathway, independently of intracellular Ca^{2+} signaling [79].

On the other hand, at high concentrations of TSH (e.g., 10 mU/mL), the TSHR predominantly activates the Gq signaling pathway through phosphatidylinositol 4,5-bisphosphate (PIP_2) hydrolysis [72], leading to activation of phospholipase C (PLC) and a subsequent increase in intracellular Ca^{2+} levels. This Ca^{2+} signaling cascade plays a crucial role in iodide organification, a process that incorporates iodide into Tg via the action of TPO. Elevated intracellular Ca^{2+} enhances H_2O_2 production, which is essential for the oxidation of iodide during hormone synthesis [79]. In addition, high Ca^{2+} levels promote Tg expression and dimerization, facilitating the assembly of thyroid hormone precursors [80]. Moreover, iodide efflux is also influenced by Ca^{2+}-dependent mechanisms [81，82], potentially mediated by Ca^{2+}-activated chloride channels, such as Anoctamin-1 (TMEM16A), which has been reported to be expressed on the apical membrane of thyrocytes [83]. This contributes to the coordinated regulation of iodide transport and efficient thyroid hormone biosynthesis.

1.2.3. Action of Thyroid hormone (TH)

In the classical genomic action of thyroid hormones (TH), TH enters the cell either by passive diffusion across the lipid bilayer or through carrier-mediated transporters. Once inside the cell, TH, particularly T3, translocate into the nucleus and bind to thyroid hormone receptors (THRs). THRs belong to the nuclear receptor superfamily and typically form heterodimers with retinoid X receptors (RXRs). These heterodimers bind to specific DNA sequences known as thyroid hormone response elements (TREs), thereby modulating the transcription of target genes, either by activating or repressing their expression in a tissue- and context-dependent manner [62].

On the other hand, thyroid hormones (THs) exert a range of non-genomic actions that occur rapidly and are mediated through membrane-associated receptors, ion channels, and signaling cascades. One well-characterized membrane receptor for TH is integrin αvβ3, which can be directly activated by TH at picomolar concentrations [84-86]. Integrin αvβ3 contains two distinct TH-binding domains, designated S1 and S2. The S1 site has a higher affinity for T3 and initiates the PI3K/Akt signaling pathway, which regulates the nuclear translocation of various proteins, including thyroid hormone receptor α (TRα). The S2 site binds both T3 and T4, but shows a higher affinity for T4, and can activate both the PI3K/Akt and MAPK cascades, thereby promoting cell proliferation [84，86]. Inhibition of TH binding to integrin αvβ3 has been shown to downregulate multiple pro-oncogenes and upregulate pro-apoptotic genes, indicating its relevance in cancer biology [84]. In addition, thyroid hormones (THs) have been shown to rapidly modulate the activity of various ion channels. For example, acute exposure (within ~5 minutes) to 10 nM T3 significantly increases tetrodotoxin (TTX)-sensitive inward Na^+ currents in cat atrial myocytes [87]. Similarly, in rat cardiac myocytes, T3 enhances the activity of inwardly-rectifying K^+ channels by increasing their open probability, indicating a direct modulatory effect on membrane excitability [88]. In addition, T3 at micromolar concentrations has been reported to directly inhibit ligand-gated ion channels, including the nicotinic acetylcholine receptor (nAChR) and the $GABA_A$ receptor [89，90]. Furthermore, T3, reverse T3 (rT3), and T4 have been shown to activate GPR35, an orphan G protein-coupled receptor (GPCR), highlighting a potential role for thyroid hormones in GPCR-mediated signaling pathways [91]. Notably, thyronamines, a class of thyroid hormone derivatives, can activate trace amine-associated receptors (TAARs), particularly TAAR1, which has been implicated in the regulation of sympathetic nervous system activity and energy metabolism [92].

1.3. Aim of the Thesis

Thyroid hormones, triiodothyronine (T3) and thyroxine (T4), primarily act through nuclear receptors to regulate the expression of target genes. However, only a limited number of studies have investigated the rapid, noncanonical actions of thyroid hormones, particularly their effects on membrane proteins, such as ion channels and G protein–coupled receptors (GPCRs).

In a preliminary screen for novel modulators of rASIC1a, it was previously observed that 1 µM L-thyroxine (T4), enhanced rASIC1a current amplitude in *Xenopus* oocytes. However, the effect of T3, the more biologically active form of thyroid hormone, remained unclear. Furthermore, it was not known whether TH affect other ASIC subunits beyond rASIC1a. The first aim of this thesis was to investigate the electrophysiological properties of various ASICs, either expressed in HEK293 cells or in *Xenopus* oocytes, to determine whether they are modulated or activated by TH, particularly T3. In addition, this study also examined endogenous ASIC expression and function in a human thyroid epithelial cell line. Finally, during the course of this work, an unexpected outward current induced by acidic pH and T3 was observed in thyroid gland cells. The second aim of this thesis was to characterize this outward current and to investigate the mechanism which triggered it.

2. Material and Methods

2.1. Materials

Reagent	Company	Solvent
3,3′,5-Triiod-L-thyronin (T2877)	Sigma-Aldrich, St. Louis, USA	DMSO
L-Thyroxine (T2376)	Sigma- Aldrich, St. Louis, USA	DMSO
3,5-Diiodo-L-thyronine	Biomol, Hamburg, Germany	DMSO
YM-254890	AdipoGen, San Diego, USA	Water
Iberiotoxin	Alomone labs, Jerusalem, Israel	Water
Amiloride	Sigma- Aldrich, St. Louis, USA	Water
Ionomycin, free acid	Calbiochem, San Diego, CA	Methanol
Gramicidin	Sigma- Aldrich, St. Louis, USA	DMSO
Fura-2 AM	Molecular Probes, Eugene, Oregon	DMSO
Pluronic F-127	Sigma-Aldrich, St. Louis, USA	-

Table 1: List of reagents and their suppliers.

The final concentration of DMSO was kept below 1 % for oocyte experiments, and below 0.1 % for cell-based experiments unless otherwise specified.

All other standard chemicals used in this study were obtained from Sigma-Aldrich (St. Louis, USA), VWR International (Pennsylvania, USA), PanReac AppliChem (Darmstadt, Germany), Carl Roth (Karlsruhe, Germany), and SERVA Electrophoresis (Heidelberg, Germany). Sterile, double-distilled water of Millipore quality was used for the preparation of solutions.

2.1.1. Cell culture media and supplements

Media/Supplement	Company
L-Glutamine (200 mM)	PAN Biotech, Aidenbach Germany
0.05% Trypsin + EDTA	Gibco, Scotland, UK
Dulbecco's Phosphate-Buffered Saline (DPBS)	PAN Biotech, Aidenbach Germany
Fetal bovine serum (FBS) Gold plus	Bio&Sell, Feucht Germany
Dulbecco's Modified Eagle Medium (DMEM)	PAN Biotech, Aidenbach Germany
Dulbecco's Modified Eagle Medium F12 (DMEM/F12)	PAN Biotech, Aidenbach Germany
Poly-D-Lysine	Sigma Aldrich, St. Louis, USA
Penicillin/Streptomycin	Sigma Aldrich, St. Louis, USA
Dimethylsulfoxide (DMSO)	Sigma Aldrich, St. Louis, USA

Table. 2: List of media and supplements for cell culture.

2.1.2. Buffers and solutions for two electrode voltage clamp (TEVC)

Component	Final concentration
NaCl	82.5 mM
KCl	2.5 mM
Na_2HPO_4	1 mM
HEPES	5 mM
PVP	0.5g/l
$MgCl_2$	1 mM
$CaCl_2$	1 mM

Table 3: OR-2 solution for incubation of *Xenopus* oocytes. The pH was 7.3 and was adjusted with NaOH.

Component	Final concentration (mM)
NaCl	140
HEPES or MES	10
$MgCl_2$	1
$CaCl_2$	1.8

Table 4: Standard bath solution for TEVC recordings. For pH from 6.7 to 7.4, HEPES buffer was used; for pH ≤ 6.7, MES buffer was used. The pH was adjusted with NaOH or HCl

2.1.3. Buffer and solutions for patch-clamp and Ca^{2+} imaging experiments.

Component	Final concentration (mM)
NaCl	128
KCl	5.4
HEPES or MES	10
$MgCl_2$	1
$CaCl_2$	2

Table 5: Standard bath solution for patch-clamp recordings of HEK cells. For pH from 6.7 to 7.4, HEPES buffer was used; for pH ≤ 6.7, MES buffer was used. The pH was adjusted with NaOH or HCl. The osmolality was adjusted to approximately 310 mOsmol/kg with glucose and measured with an Osmometer.

Component	Final concentration (mM)
NaCl	10
KCl	121
EGTA	5
$MgCl_2$	2
HEPES	10

Table 6: Pipette solution for whole cell patch-clamp recordings of HEK cells. The pH was 7.2 and was adjusted with NaOH and the osmolality was adjusted to approximately 280 mOsmol/kg.

Component	Final concentration (mM)
NaCl	115
KH_2PO_4	0.4
K_2HPO_4	1.6
Glucose	5
$MgCl_2$	1
HEPES or MES	5
Na-Gluconat	25
Ca-Gluconat	3

Table 7: Ringer bath solution for whole-cell recordings and Ca^{2+} imaging of Nthy-ori-3-1 cells. For pH from 6.7 to 7.4, HEPES buffer was used; for pH ≤ 6.7, MES buffer was used. The pH was adjusted with NaOH or HCl. The osmolality was between 280 - 310 mOsmol/kg.

Component	Final concentration (mM)
K-Gluconat	95
KCl	30
NaH_2PO_4	1.2
Na_2HPO_4	4.8
Glucose	5
$MgCl_2$	2.38
EGTA	1
Ca-Gluconat	0.726
ATP	3

Table 8: Pipette solution for whole cell patch-clamp recordings of Nthy-ori-3-1 cells. The pH was 7.2 and adjusted with NaOH. The osmolality was approximately 245 mOsmol/kg

Component	Final concentration (mM)
NaCl	115
KH_2PO_4	0.4
K_2HPO_4	1.6
Glucose	5
$MgCl_2$	1
HEPES or MES	5
Na-Gluconat	25
EGTA	5

Table 9: Ringer Ca^{2+} free bath solution for whole-cell recordings of Nthy-ori-3-1 cells.

Component	Final concentration (mM)
NMDG	140
KH_2PO_4	0.4
K_2HPO_4	1.6
Glucose	5
$MgCl_2$	1
HEPES or MES	5
Ca-Gluconat	3

Table 10: Ringer NMDG bath solution for whole-cell recordings of Nthy-ori-3-1 cells.

Component	Final concentration (mM)
NaCl	115
KH_2PO_4	0.8
K_2HPO_4	3.2
Glucose	5
$MgCl_2$	1
HEPES or MES	5
Na-Gluconat	25
EGTA	5

Table 11: Erev(K) Ringer bath solution for whole-cell recordings of Nthy-ori-3-1 cells with $E_{rev(K+)}$ = -70 mV.

2.1.4. Laboratory devices

Device	Company
Metrohm 827 pH-meter	pH lab
Magnet stirrer	Heidolph, Schwabach, Germany
Pipettes (2 µl, 10 µl, 20 µl, 100 µl, 200 µl, 1 ml)	Eppendorf, Hamburg, Germany
Microscale XA205 Dual Range	Mettler Toledo, Columbus, USA
Osmometer Osmomat 030	Genotec, Waiblingen, Germany
Millipore Advantage 10	Milli-Q, Darmstadt, Germany
Pipetboy 2	Integra, Zizers, Switzerland
T3000 Thermocycler	Biometra, Göttingen, Germany
Centrifuge	Eppendorf, Hamburg, Germany
Vortex Genie	Eppendorf, Hamburg, Germany
Water Bath	GFL, Burgwedel, Germany
CO_2 Incubator	Binder, Tuttlingen, Germany
Axiovert 25 microscope	Zeiss, Oberkochen, Germany
Binocular microscope Stemi DV4	Zeiss, Oberkochen, Germany
HBO50 Fluorescence Lamp	Osram, Munich, Germany
DMZ Universal Puller	Zeitz, Bavaria, Germany
Patch Clamp	
cFlow Perfusion system	Cell MicroControls, Virginia, USA
Light microscope	Olympus, Tokyo, Japan
DMZ Universal Electrode Puller	Zeitz, Bavaria, Germany
SM-5 Micromanipulator	Luigs & Neumann, Ratingen Germany
Analog-digital converter Digidata 1440A	AXON CNS Molecular devices, California, USA
MultiClamp 700B	AXON CNS Molecular devices, California, USA
Glass capillary tube for patch clamp (GC120TF-10)	Harvard apparatus, Massachusetts, USA
TEVC	
Flaming/Brown Micropipette Puller (Model P-97)	Sutter Instrument, California, USA
Stemi 2000-C microscope	Zeiss, Oberkochen, Germany

Rotamax 120 platform shaker	Heidolph Instruments, Schwabach, Germany
Nanoject II Injector	Drummond scientific company, Pennsylvania, USA
Oocyte-testing carrousel	npi electronic, Württemberg, Germany
Turbo Amplifier TEC-03X	Turbo Technics, NN4 7PL UK
KL1500 LCD lamp	Zeiss, Oberkochen, Germany
Glass capillary tube for TEVC (GB150TF-10)	
Ca^{2+} Imaging	
SM-7 Micromanipulator	Luigs & Neumann, Ratingen Germany
Light microscope (IX71)	Olympus, Hamburg, Germany
Pump	ISMATEC, Grevenbroich Germany
Polychrom V	LabWrench, Midland, ON, Canada
Image Control unit	TILL Photonics, Martinsried Germany
Sensicam CCD camera	PCO imaging, Kelheim, Germany
cFlow Perfusion system	Cell MicroControls, Virginia USA

Table 12: List of laboratory devices.

2.1.5. Plasmid vectors

Plasmid	Origin
rASIC1a pRSSP	Gründer lab
rASIC3 pcDNA3.1	Gründer lab
hASIC1a pRSSR6013	Gift by G. Schmalzing, Aachen
hASIC3b pRSSP	Gift by G. Schmalzing, Aachen

Table 13: List of used plasmids in this project. pRSSP is an oocyte expression vector, based on the plasmid pSP64, additionally containing the 5´UTR of Xenopus b-globin and a poly-A tail.

2.1.6. Software

Software	Company
Clampex	Molecular Devices, California USA
ClampFit	Molecular Devices, California USA
Till Vision real-time imaging software	T.I.L.L.Photonics, Bavaria Germany
CellWorks 6.1.2.	npi electronic, Württemberg Germany
CellWorks Reader 6.2.2.	npi electronic, Württemberg Germany
Prism	GraphPad, Massachusetts USA
Adobe Illustrator 2023	Adobe, California USA
IgorPro	Wave Metrics, Oregon USA
Microsoft Office	Microsoft, Washington USA

Table 14: List of software.

2.2. Methods

2.2.1. TEVC (Two electrode voltage clamp)

In this thesis, two-electrode voltage clamp (TEVC) was employed to characterize the biophysical properties of cell membranes and ion channels in *Xenopus laevis* oocytes. The *Xenopus* oocyte expression system is one of the most widely used models for TEVC recordings. In this system, the cRNA of the target ion channel is microinjected into the oocyte, which then expresses the exogenous protein. As *Xenopus laevis* oocytes express only a limited number of endogenous ion channels, the functional characterization of heterologously expressed channels is minimally affected by background activity. This makes the system ideal for studying the biophysical properties and ligand sensitivity of specific ion channels.

Stage V–VI oocytes were surgically harvested from adult *Xenopus laevis* females under anesthesia with tricaine methanesulfonate (2.5 g/l for 20 minutes). After the final oocyte harvest, frogs were euthanized by decapitation. Ovarian lobes were dissected into small fragments using forceps and incubated in collagenase solution (25 mg/ml) for approximately 2 hours to enzymatically remove the follicular layer and facilitate separation of individual oocytes. Following digestion, oocytes were washed four to five times with OR-2 medium to eliminate residual collagenase and tissue debris. All animal care and experimental procedures were approved by the State Office for Nature, Environment and Consumer Protection of North Rhine-Westphalia (LANUV NRW; approval # 81-02.04.2019.A356).

Healthy oocytes were selected based on morphological criteria, including a well-defined animal–vegetal polarity and an intact, undamaged membrane. Selected oocytes were microinjected with 42 nl of cRNA encoding the desired ASIC using a calibrated microinjector. The injected oocytes were incubated at 19 °C in OR2 medium for one to two days, with daily medium replacement.

The TEVC setup consisted of several key components. The experimental chamber (Fig. 4) was used to hold the oocyte in position using gentle negative pressure, enabling stable insertion of both the potential and current electrodes. An automated perfusion system, consisting of an oocyte testing carousel and pump, was employed to enable fast solution exchange.

Whole-cell currents were recorded with a TurboTec 03X amplifier (Table 12; Fig. 5) using GB150TF-10 glass pipettes (1.05 x 1.50 x 100 mm). Data were acquired at a sampling rate of 200 Hz using CellWorks software, and current traces were visualized with CellWorks Reader

software. Unless otherwise specified, all recordings were performed at a holding potential of –70 mV. Experiments were conducted at room temperature (20–25 °C).

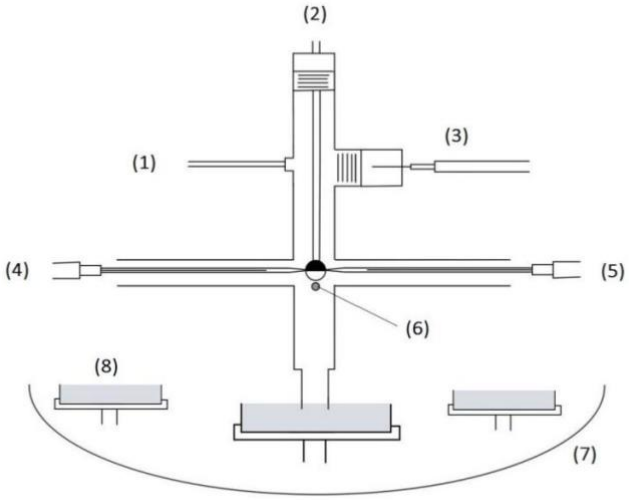

Figure 4: Experimental chamber for the fast solution exchange system. 1: Pump; 2: Capillary to fix the oocyte; 3: Reference electrode; 4: Potential electrode; 5: Current electrode; 6: Ground electrode; 7: Carousel; 8: containers for different solutions

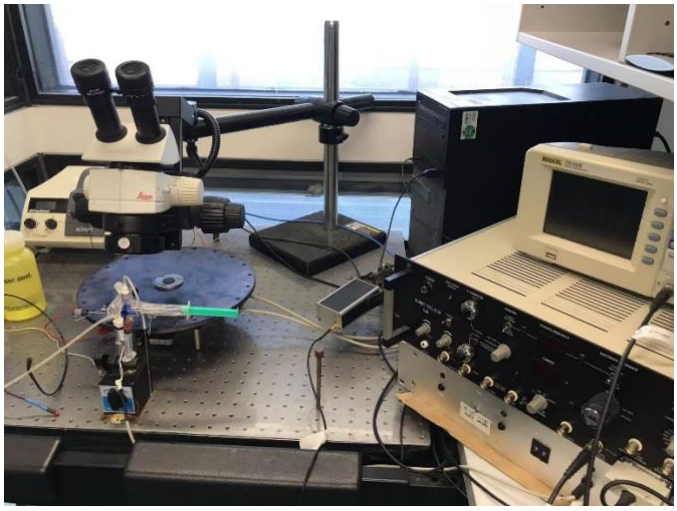

Figure 5: Overview of the TEVC setup

2.2.2. Cell culture

In this thesis, two cell types were used: human embryonic kidney (HEK) 293 *Asic1*$^{-/-}$ cells and normal human thyroid follicular epithelial cells (Nthy-ori-3-1).

Cell line	Origin
Human embryonic kidney (HEK 293) cells (*Asic1*$^{-/-}$)	Gift by S. Pless; Copenhagen
Nthy-ori-3-1 cells	Gift by P. Caria; Cagliari

Table 15: List of cell lines.

HEK 293 cells were cultivated in Dulbecco's Modified Eagle Medium (DMEM) supplemented with 10 % fetal bovine serum (FBS), while Nthy-ori-3-1 cells were maintained in DMEM/F12 supplemented with 10 % FBS and 1 % L-glutamine, both in standard 10 cm culture dishes. Cells were passaged every 2 – 4 days, when confluence reached approximately 90 %.

For passaging, cells were washed with 5 ml phosphate-buffered saline (PBS), followed by incubation with 1 ml of 0.05 % trypsin to detach the cells. HEK cells were incubated at room temperature for ~1 minute, while Nthy-ori-3-1 cells were incubated at 37 °C for ~ 1 minute. After detachment, 5 ml of complete culture medium was added to neutralize the trypsin. The cell suspension was then centrifuged at 1,200 rpm for 90 seconds, and the supernatant was discarded. The cell pellet was resuspended in 1 ml of medium and seeded either into 10 cm dishes for continued maintenance or into 2 cm dishes for experimental use.

To study the electrophysiological properties of exogenous rASIC3, HEK 293 cells were transiently transfected with a total of 1–2 µg/ml of plasmid DNA using 6–8 µg of polyethylenimine (PEI). The transfection mixture consisted of rASIC3 cDNA (0.5–1 µg/ml) and an equal amount of GFP-expressing plasmid (pcDNA-GFP) to facilitate identification of successfully transfected cells. Plasmids were diluted in 150 µl of serum-free medium, vortexed, and mixed with PEI. After incubation at room temperature for 30 minutes to allow polyplex formation, the transfection mix was added dropwise to the culture dish, followed by gentle rocking. After 24 hours, the medium was replaced, and cells were replated onto glass coverslips pre-coated with 0.01 % poly-D-lysine for subsequent patch-clamp recording.

In contrast, Nthy-ori-3-1 cells, used to study endogenous channels and receptor activity, were not transfected. Instead, they were directly seeded onto poly-D-lysine-coated coverslips and used for patch-clamp electrophysiology and Ca^{2+} imaging experiments.

2.2.3. Patch clamp technique

In this thesis, whole-cell currents were recorded using the patch-clamp technique with an Axon MultiClamp 200B amplifier (Table 12). Data acquisition was performed using the Axon Digidata 1440A digitizer, controlled via Clampex 10.0 software (pClamp 10.0, Molecular Devices, Sunnyvale, CA, USA). Signals were sampled at 10 kHz and low-pass filtered at 0.4 kHz. Unless otherwise indicated, the holding potential was maintained at −70 mV throughout all experiments.

Glass micropipettes (1.2 mm OD × 0.94 mm ID × 100 mm length) were pulled using a DMZ Universal Electrode Puller. Pipette resistances ranged from 3 – 5 MΩ for HEK 293 cell recordings and 4 – 9 MΩ for Nthy-ori-3-1 cell recordings. Pipettes were prepared immediately prior to experiments and used on the same day to ensure optimal quality.

Whole-cell patch-clamp measurements were carried out according to the method initially established by Neher and Sakmann [93]. Coverslips containing either ASIC-transfected HEK293 cells or Nthy-ori-3-1 cells were placed in the recording chamber.

Cell selection criteria were as follows: 1. For HEK 293 cells, selected cells had to be well separated, firmly attached to the coverslip, and exhibit moderate GFP fluorescence, which served as an indicator of successful ASIC expression. 2. For Nthy-ori-3-1 cells, recordings were performed only on cells exhibiting clear membrane borders and a membrane capacitance between 20–50 pF, to ensure the current originated from a single cell and that the cell size was optimal for patch-clamp recording.

Patch pipettes were filled with internal solution (see Table 8) and carefully approached to the cell membrane. Upon contact, a slight increase in resistance (5–10 MΩ) was monitored. A gentle negative pressure was then applied to establish a giga-seal (>1 GΩ). Following seal formation, a brief but stronger suction was applied to rupture the membrane and achieve the whole-cell configuration.

Cells exhibiting a stable leak current of < 200 pA were accepted for HEK 293 recordings. For Nthy-ori-3-1 cells, a higher leak current threshold of < 500 pA was tolerated, due to the presence of constitutively active channels.

The osmolality of both bath and internal pipette solutions was adjusted using glucose. Bath solution osmolality was maintained between 280–300 mOsm/kg, while the internal pipette

solution was adjusted to be approximately 30 mOsm/kg lower than the bath, to promote cell stability during recordings.

2.2.4. Ratiometric Ca^{2+} Imaging

Fura-2 was used to monitor changes in intracellular Ca^{2+} concentration $[Ca^{2+}]_i$. Fura-2 is a ratiometric, UV-excitable fluorescent dye that forms chelate complexes with Ca^{2+} ions, allowing the quantification of Ca^{2+} dynamics within live cells.

Upon binding to Ca^{2+}, Fura-2 exhibits a shift in its excitation spectrum, with excitation peaks at 340 nm (Ca^{2+}-bound) and 380 nm (Ca^{2+} -free). Fluorescence emission is measured at approximately 510 nm, where the intensity of the signal is directly correlated with intracellular Ca^{2+} levels. The ratio of fluorescence intensity at the two excitation wavelengths (F_{340}/F_{380}) allows for accurate and reliable estimation of intracellular Ca^{2+} concentrations, independent of dye concentration or cell thickness.

Fluorescence imaging was recorded every 5 s and performed using a Fluar 20×/0.75 objective; data were acquired using TillVision real-time imaging software (see Table 12). All measurements were conducted under controlled conditions and standardized exposure settings.

Ca^{2+} imaging was performed as previously [94]. To prepare the dye-loading solution, 4 µl of Fura-2 AM stock solution (1 mM in DMSO) was mixed with 1.25 µl of Pluronic F-127 stock solution (20 % in DMSO) in a 1.5 ml Eppendorf tube. This mixture was then diluted with 1 ml of Ringer standard bath solution (see Table 7) to achieve a final Fura-2 AM concentration of 4 µM.

Nthy-ori-3-1 cells, previously seeded on glass coverslips, were twice gently rinsed with Ringer solution. The Fura-2/Pluronic F-127 solution was then applied to the cells, and the coverslips were incubated for 30 minutes at 37 °C in the dark to allow for dye uptake. After incubation, the loading solution was removed, and the cells were rinsed with 2 ml of Ringer solution, followed by incubation in 1 ml of fresh Ringer solution for an additional 15 minutes at room temperature in the dark. This step permitted intracellular esterases to cleave the AM ester groups, thereby trapping the active dye within the cytosol. Following dye de-esterification, the coverslips were transferred to a recording chamber for Ca^{2+} imaging. The solutions and perfusion conditions used during imaging were identical to those described for the whole-cell patch-clamp experiments.

2.2.5. Data analysis

TEVC recordings were obtained from *Xenopus* oocytes derived from at least two different animals to ensure reproducibility. Patch-clamp experiments were performed on at least two independent recording days, each involving separate transfections. Ca^{2+} imaging data were collected from a minimum of three independent recording sessions conducted on different days.

Data were analysed using the software IgorPro, Prism 9 and ClampFit 10.1. Results are reported as the mean ± S.E.M.; individual data points are shown on the figures to allow assessment of their variation. Normal distribution of the data was assessed using Shapiro-Wilk test. For normally distributed data, statistical significance was assessed using one-way ANOVA, unpaired and paired Student's t-test, as appropriate. For data that did not follow a normal distribution, the Kruskal–Wallis test was used instead of one-way ANOVA, and the Mann–Whitney U test instead of the t-test.

Concentration - response curves were fitted to a Hill function.

$$I_x = \frac{1}{1 + (\frac{[x]}{IC50})^H}$$

where I_x is the current at a given compound concentration, $[x]$ is the concentration of the compounds, IC_{50} is the concentration at which 50 % of the current was inhibited or potentiated, and H represents the Hill coefficient.

3. Results

3.1. The effect of thyroid hormone (TH) on the biophysical properties of rat ASIC1a

3.1.1. rat ASIC1a currents are potentiated by T2, T3 and T4.

In a previous preliminary screen for novel compounds that modulate rASIC1a, it was observed that 1 mM L-thyroxine (thyroid hormone; T4) increased the current amplitude of rASIC1a in *Xenopus laevis* oocytes.

To investigate this effect in more detail, we performed experiments using rASIC1a-expressing oocytes and measured currents at pH 6.5. This pH was selected because it activates approximately 50 % of rASIC1a channels, providing a dynamic range to detect potentiation, and at the same time minimizing tachyphylaxis, a phenomenon where repeated activation leads to reduced current amplitudes [95].

Application of 1 µM T4 at pH 6.5 did not significantly potentiate rASIC1a currents. However, sustained application (application prior to and during ASIC1a activation) of 10 µM T4 significantly increased the typical transient current amplitude 1.55 ± 0.11-fold ($P = 0.0008$; Fig. 6B).

In addition to T4, the biologically active thyroid hormone T3 (triiodothyronine, Fig.6A), as well as the less active metabolite T2 (diiodothyronine, Fig.6A), also significantly potentiated rASIC1a currents during sustained application. Application of 20 µM T2 enhanced current amplitude 1.56 ± 0.09-fold ($P = 0.0007$; Fig. 6B), comparable to the effect of T4. Notably, 20 µM T3 potentiated the current 3.01 ± 0.14-fold ($P < 0.0001$; Fig. 6B), indicating a substantially stronger potentiation.

To evaluate the concentration dependence of ASIC1a potentiation by TH, we applied T2, T3, and T4 at concentrations ranging from 100 nM to 20 µM before and during pH 6.5 application. The potentiation was concentration-dependent, increasing with rising concentrations. All three TH exhibited similar EC_{50} values in the low micromolar range: T2 exhibited an EC_{50} of 6.3 ± 1.34 µM (n = 6 - 7), T3 of 4.5 ± 4.47 µM (n = 8–10), and T4 of 2.8 ± 3.04 µM (n = 10; Fig. 6C).

These findings demonstrate that TH, particularly T3, can potentiate rASIC1a currents and may function as novel endogenous modulators of rASIC1a activity.

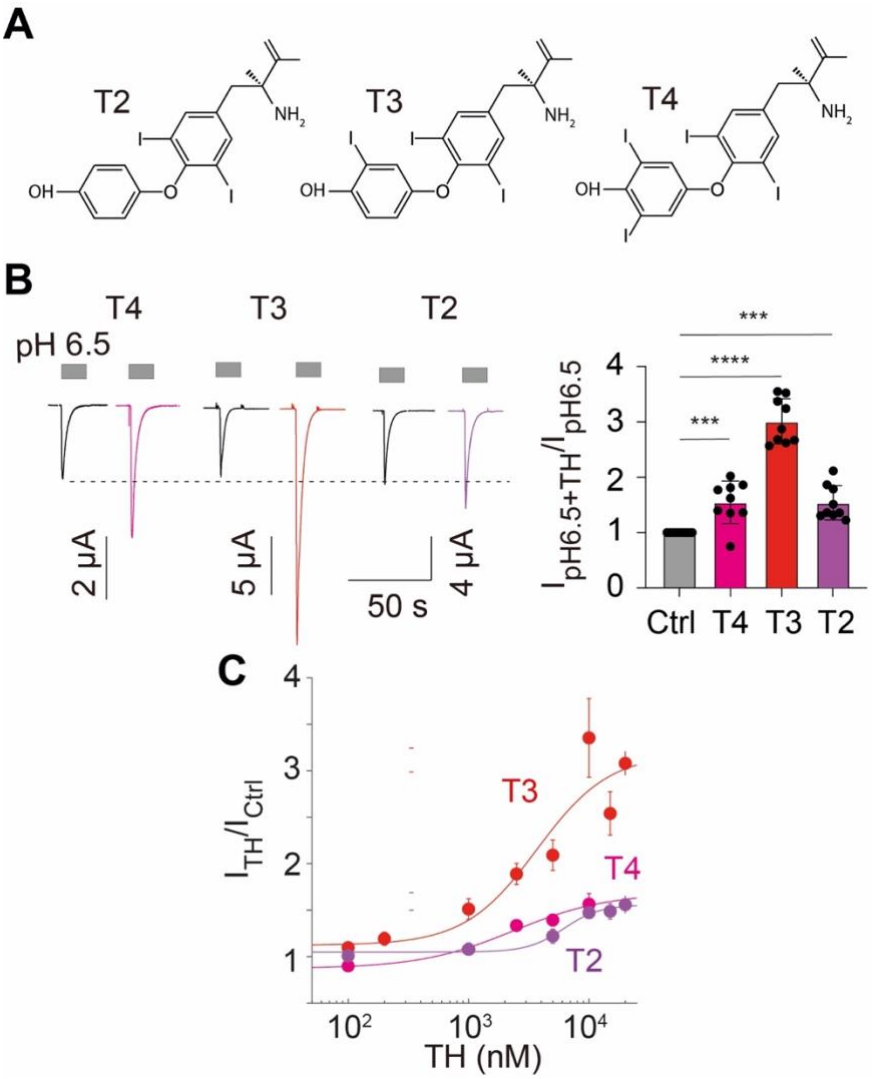

Figure 6. Thyroid hormones potentiate ASIC1a currents in *Xenopus* oocytes. **(A)** Structure of diiodothyronine (T2), triiodothyronine (T3) and thyroxine (T4). **(B)** Left, representative current traces of an rASIC1a-expressing oocyte. rASIC1a was activated by pH 6.5 in the absence or presence of 20 µM T2 (n = 10), 20 µM T3 (n = 9), or 10 µM T4 under sustained application conditions (n = 10). Right, quantitative analysis of peak currents. **(C)** Concentration-response curves for T2, T3, and T4 on ASIC1a; n = (5-10). rASIC1a was activated by pH 6.5 with increasing T3 concentrations; TH were pre- and co-applied with pH 6.5. The curves represent fits to the Hill equation. Dots represent the mean and error bars the SEM. ***, $P < 0.001$; ****, $P < 0.0001$.

3.1.2. T3 rapidly binds to and unbinds from rat ASIC1a

Due to its highest efficacy among the tested TH, T3 was selected for further investigation in subsequent experiments. In the experiments reported in Figure 6, T3 was applied in a sustained manner to assess its full potentiating effect. To further evaluate the onset kinetics and potential state-dependent binding, we also examined the effects of T3 under two additional application paradigms: pre-application and co-application.

Both pre-application and co-application of 20 μM T3 reversibly potentiated rASIC1a currents. Co-application of T3 resulted in a 2.7-fold increase in current amplitude, comparable to the effect observed with sustained application (P = 0.78; Fig. 7A and 7B). In contrast, pre-application of T3 produced only a 1.7-fold potentiation, which was significantly smaller (P = 0.002 vs. co-application; P = 0.0001 vs. sustained application; Fig. 7A and 7B). These findings suggest that the onset of T3 action is very rapid (on the order of milliseconds) and that T3 preferentially interacts with rASIC1a channels in their open rather than closed conformational state or that T3 rapidly unbinds.

In addition to its rapid onset, T3-induced potentiation also exhibited rapid reversibility upon washout. To investigate the dissociation kinetics of T3, we applied T3 at pH 7.4, followed by washout and subsequent activation of ASIC1a at various time points after wash-out (0, 5, 10, 15, and 60 s). The potentiation was significantly reduced within the first 5 seconds of washout (from 1.73- to 1.43-fold; P = 0.041; Fig. 7C), but no further decrease was observed with extended washout up to 60 seconds (P = 0.97; Fig. 7C), indicating that T3 partially dissociates within seconds from the closed state of rASIC1a.

Interestingly, when ASIC1a was activated during the washout phase, the T3 potentiation was completely abolished after 60 s (P = 0.471; Fig. 7D), suggesting that activation accelerates dissociation of T3. Collectively, these results imply that T3 can bind to rASIC1a in both the closed and open conformations. Moreover, in the open or desensitized state, T3 dissociates more rapidly and completely.

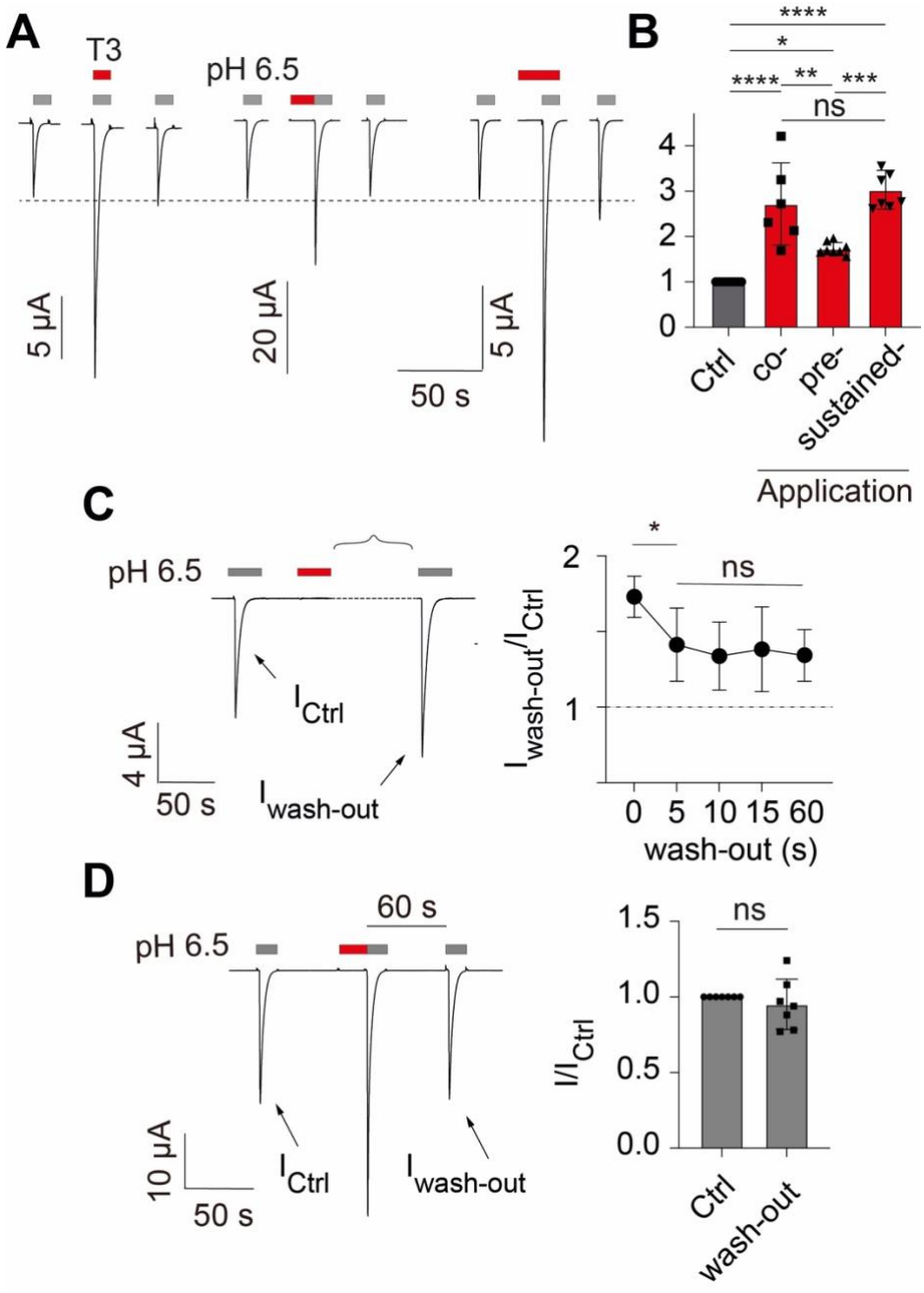

Figure 7. Effect of T3 on rASIC1a currents in *Xenopus* oocytes under pre-, co-, and sustained application. **(A)** Representative current traces of rASIC1a, activated by pH 6.5; 20 µM T3 was pre-, co- or pre- and co-applied (sustained). **(B)** Quantitative analysis of peak currents. Currents were normalized to the peak before T3 application (n = 7). **(C)** Left, rASIC1a was activated by pH 6.5, 20 µM T3 was applied and washed out for different times (0, 5, 10, 15, or 60 s), followed by a second activation with pH 6.5. Right, quantitative analysis of peak currents after washout of T3, normalized to the current before T3 application (n = 7). **(D)** Left, representative current trace of rASIC1a activated by pH 6.5 immediately after T3 application and 60 s after wash-out of T3. Right, quantitative analysis of peak currents before T3 application and 60 s after washout (n = 7). Bars represent mean ± SEM. ns, not significant; *, $P < 0.05$; **, $P < 0.01$; ***, $P < 0.001$; ****, $P < 0.0001$.

3.1.3. T3 increases the efficacy of protons to activate rat ASIC1a

The potentiation of rASIC1a by T3 has been clearly demonstrated; however, the underlying mechanism remained unclear. In general, potentiation of ion channels may result from various mechanisms, including: changes in membrane properties that indirectly modulate channels; increased expression or trafficking of channels to the membrane; enhanced proton affinity; increased proton efficacy.

It has been previously reported that certain amphiphilic compounds can modulate ASICs or ASIC-related channels (e.g., BASIC) by altering membrane properties. As an amphiphilic molecule, T3 might also influence membrane characteristics and indirectly affect ASIC activity [61]. To address this possibility, we assessed the effect of T3 on leak currents mediated by gramicidin A (gA), a small peptide that forms ion channels embedded within the lipid bilayer. Because gA function is sensitive to changes in membrane properties, it serves as a reliable reporter. We applied 20 μM gA to oocytes, followed by superfusion with bath solutions containing 0.4 % DMSO (vehicle), 20 μM T3, or 25 μM TA (a positive control; Fig. 8A). As expected, TA significantly reduced gA-induced currents. In contrast, neither DMSO nor T3 altered the current amplitude, indicating that T3 does not affect membrane physical properties of oocytes.

To investigate whether T3 modulates the proton sensitivity of ASIC1a, we recorded the pH activation curve of rASIC1a in the presence and absence of 20 μM T3 (Fig. 8B). In the absence of T3, the pH_{50} was 6.66 ± 0.03, with maximal activation occurring at pH 6.0. In the presence of T3, the pH_{50} was 6.61 ± 0.03, which was not significantly different from control ($P = 0.242$), indicating that T3 does not alter the proton affinity of rASIC1a.

In agreement, when T3 was applied at pH 6.0, a condition under which the channel is typically fully activated, T3 still significantly potentiated rASIC1a currents (Fig. 8D). This suggests that T3 increases the efficacy, rather than the potency, of protons in activating ASIC1a.

To examine whether T3 alters ion selectivity, we measured the reversal potential (E_{rev}) in the presence and absence of T3 (Fig. 8C). Under control conditions, E_{rev} was 25.3 ± 1.9 mV, and in the presence of T3, it was 24.8 ± 1.9 mV ($P = 0.856$), indicating that T3 does not affect the ion selectivity of rASIC1a.

Taken together, these results show that T3 does not affect membrane properties, proton sensitivity, or ion selectivity, and due to its rapid onset kinetics, an increase in channel expression at the membrane is also unlikely. Notably, T3 was able to potentiate the current amplitude even under fully activating proton conditions. These findings support the conclusion that T3 enhances rASIC1a current by increasing proton efficacy, most likely by increasing the open probability P_o at a given proton concentration.

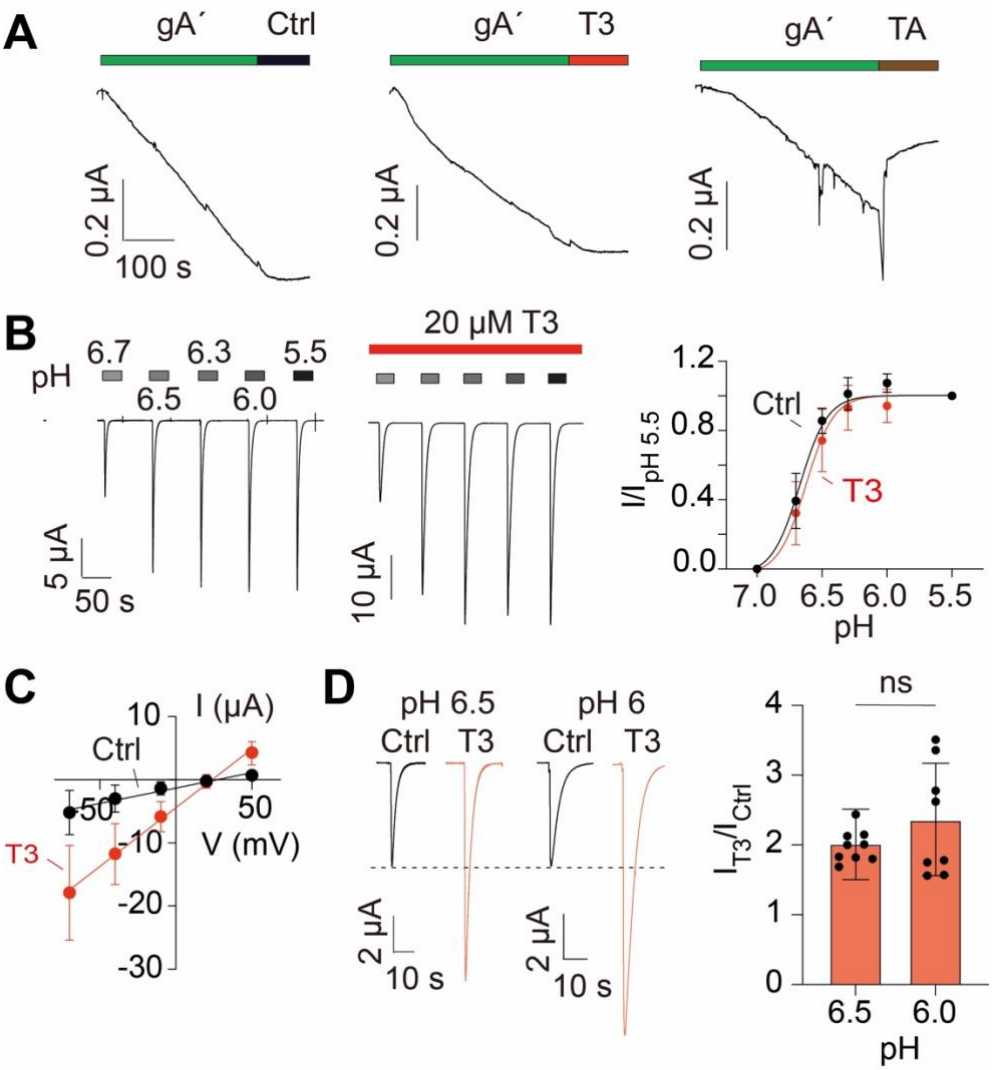

Figure 8. Exploring the potentiation mechanism of T3 on rASIC1a. (A) Representative current traces of un-injected oocytes, treated with 20 µM gramicidin A (gA) and subsequent application of 0.4 % DMSO (ctrl, left), 20 µM T3 (middle), or 25 µM tannic acid (TA, right). **(B)** Left, representative current traces of rASIC1a, repeatedly activated by different proton concentrations in the absence (left) or presence (right) of 20 µM T3. Right, pH dependence of ASIC1a in the presence or absence of 20 µM T3; curves represent fits to the Hill equation (n = 8). **(C)** Mean current-voltage (I-V) relationships of rASIC1a-expressing oocytes recorded in the presence or absence of 20 µM T3. The holding potential was continuously increased from −70 to +50 mV within 1 s (n = 12). **(D)** Left, Representative current traces of rASIC1a, elicited by pH 6.5 or pH 6.0 in the presence or absence of 5 µM T3. Right, quantitative analysis of peak currents. Bars represent mean ± SEM. ns, not significant.

3.2. The effect of the thyroid hormone T3 on the biophysical properties of rat ASIC3

3.2.1. T3 potentiates transient rat ASIC3 currents and induces sustained currents

Having established the effect of T3 on rASIC1a, we next sought to determine whether this effect is specific to rASIC1a or also applies to other ASIC subtypes. To this end, we investigated the influence of T3 on rASIC3. Because of the more rapid desensitization kinetics of ASIC3 and because TEVC measurements are not suitable for recording rapid responses, we heterologously expressed rASIC3 in HEK 293 cells and assessed its electrophysiological properties using whole-cell patch clamp recordings.

As with rASIC1a, we examined the effect of T3 using three different application paradigms: co-, pre-, and sustained application (Fig. 9A). rASIC3 was activated by pH 6.7, which corresponds to its pH_{50}. In the presence of 10 µM T3, the amplitude of the transient rASIC3 current was approximately 2-fold potentiated under all three conditions ($P_{\text{co-application}} = 0.0046$; $P_{\text{pre-application}} = 0.0029$; $P_{\text{sustained application}} = 0.0004$; Fig. 9B). This potentiation was reversible within < 10 seconds following washout. Notably, in addition to potentiating the transient rASIC3 current, T3 induced a small sustained current following the transient peak response at pH 6.7 (Fig. 9A, left, inset). Interestingly, a similarly small, sustained current was also observed when T3 was applied alone at neutral pH 7.4 (Fig. 9A, right, inset), suggesting a direct activating effect independent of acidification.

To further characterize these T3-induced sustained currents, we co-applied the Deg/ENaC pore blocker amiloride (100 µM) and T3 under both neutral and acidic pH conditions (Fig. 9C). Consistent with our initial observations, T3 elicited sustained inward currents in both conditions. These responses were not detected in non-transfected cells, confirming their specificity to rASIC3 expression. Interestingly, the T3-induced sustained current at neutral pH was significantly enhanced by amiloride, whereas the current observed under acidic pH remained unaffected. These contrasting effects suggest that T3 activates two mechanistically distinct types of sustained rASIC3 currents. It has been reported that low concentrations of amiloride (e.g., 100 µM) can potentiate the ASIC3 window current [43]. Therefore, the sustained current observed under neutral pH likely reflects a potentiated window current. In contrast, the sustained current under acidic conditions may represent an enhancement of a non-desensitizing current component typically induced only by very acidic pH [43].

In summary, T3 not only potentiated the transient, proton-activated current of rASIC3, but also induced a sustained current under both neutral and acidic pH conditions, suggesting a more complex modulatory role of T3 on ASIC3 function.

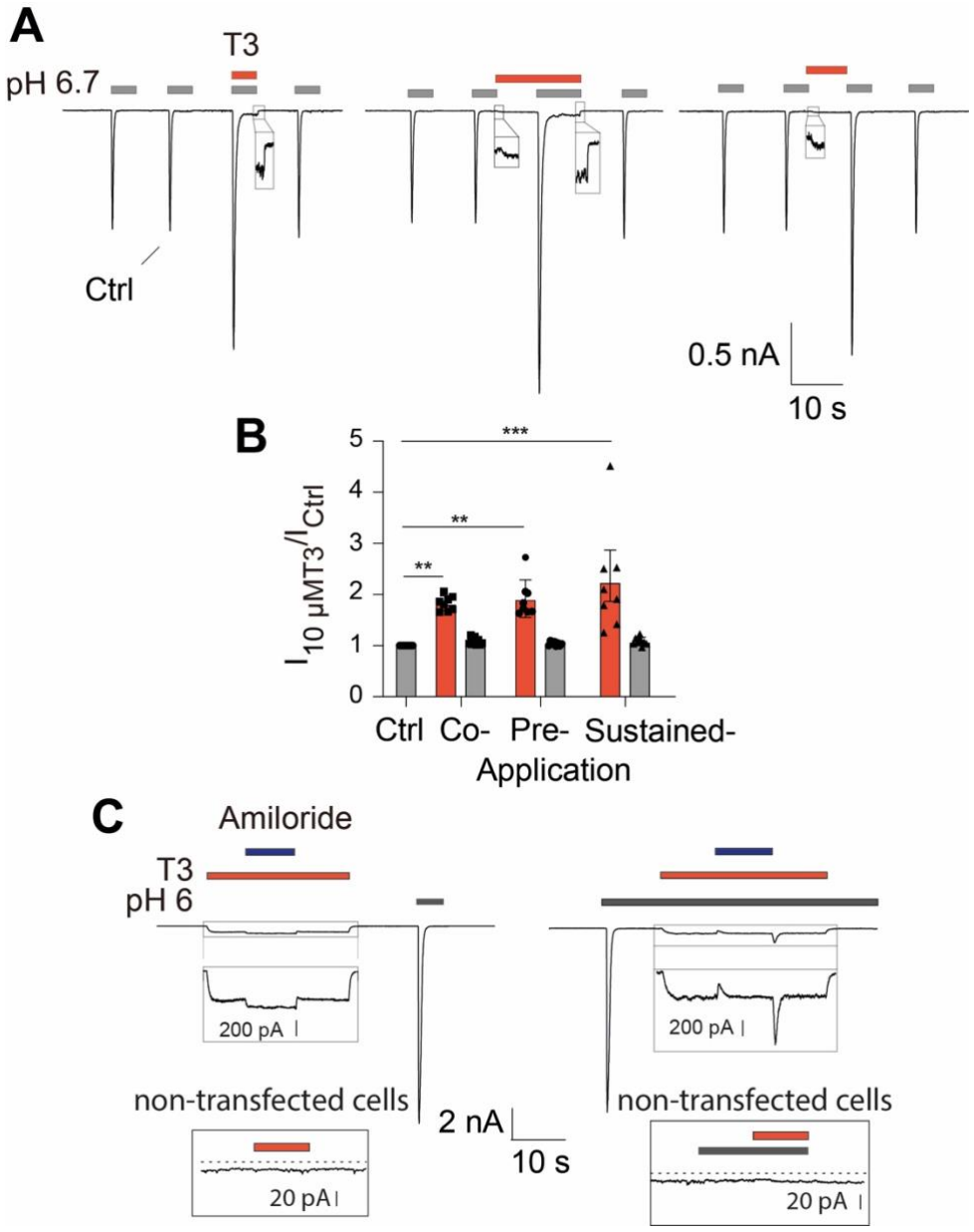

Figure 9. The thyroid hormone T3 potentiates rASIC3 currents under pre-, co- and sustained application. **(A)** Representative current traces of HEK 293 cells expressing rASIC3. rASIC3 was repeatedly activated by pH 6.7 in the absence or presence of 10 µM T3. Left, co-application of T3, middle, pre-application of T3, right, pre- and co-application (sustained application) of T3. **(B)** quantitative analysis of rASIC3 peak currents under different conditions of T3 application. Currents were normalized to the peak before T3 application. Currents after wash-out of T3 are also shown (n = 8). **(C)** Current traces representative for 4 similar measurements illustrating the effect of 100 µM amiloride on rASIC3 exposed to 10 µM T3 at pH 7.4 (left) or pH 6.0 (right). The inset shows a representative trace of a non-transfected cell in presence of T3 at pH 7.4 and pH 6.0 (n = 4). Bars represent mean ± SEM. **, $P < 0.01$; ***, $P < 0.001$.

3.2.2. T3 increases the proton sensitivity of rat ASIC3

Similar to rASIC1a, T3 also potentiated rASIC3 currents at micromolar concentrations. To explore the concentration-response relationship, we applied T3 at concentrations ranging from 1 nM to 10 μM at two different pH values: pH 6.0 and pH 7.0.

At pH 6.0, where rASIC3 is fully activated, T3 failed to potentiate the transient current. However, the sustained current was significantly enhanced by T3 in a concentration-dependent manner (Fig. 10A). Additionally, the desensitization time constant (τ) was significantly increased in the presence of T3 compared to control (P = 0.030), indicating that T3 slows the desensitization kinetics of rASIC3 (Fig. 10A).

In contrast, at pH 7.0, where the window current occurs, T3 robustly potentiated both transient and sustained rASIC3 currents in a concentration-dependent manner (Fig. 10B). Notably, this potentiation did not reach saturation even at the highest T3 concentration tested (10 μM). These findings suggest that, unlike its effect on rASIC1a, T3 enhances the proton sensitivity of rASIC3 without altering proton efficacy. Moreover, these results further indicate that T3 enhances both window and acid-induced sustained currents in rASIC3.

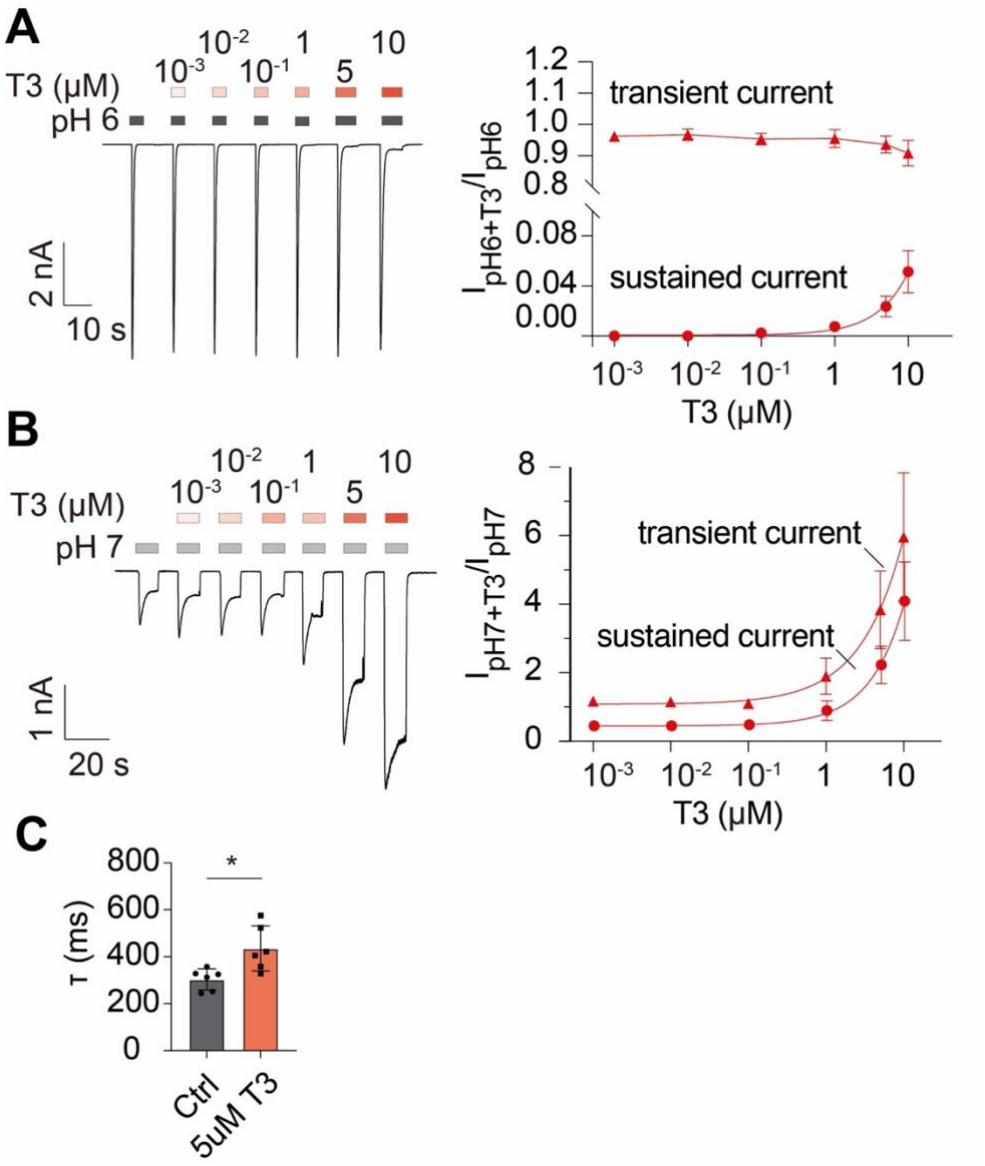

Figure 10, Concentration-response curve for the potentiation of rASIC3 by T3. (A) Left, representative current traces of rASIC3, repeatedly activated by pH 6.0 in the presence of increasing concentrations of T3. Right, concentration-response curves. Currents were normalized to the transient current in the absence of T3. Curves represent fits to the Hill function (n = 8). (B) Left, representative current trace of rASIC3 repeatedly activated by pH 7.0 in the presence of increasing concentrations of T3. Right, concentration-response curves. Currents were normalized to the transient current in the absence of T3. Curves represent fits to the Hill function (n = 8). **(C)** Comparison of the time constant τ for desensitization of rASIC3 recorded at pH 6 in the presence and absence of 5 μM T3. Bars represent mean ± SEM. *, $P < 0.05$.

3.2.3. T3 shifts activation and SSD curves of rat ASIC3, increasing the window current

To further investigate whether T3 altered the proton sensitivity of rASIC3, we recorded both the activation and steady-state desensitization (SSD) curves in the absence and presence of 5 μM T3 (Fig. 11A and 11B). In the control condition, rASIC3 currents increased progressively as pH decreased from 7.2 to 5.5, reaching saturation at pH 6.0, with a pH_{50} of 6.67 ± 0.03. In the presence of T3, saturation occurred already at pH 6.6, and the pH_{50} shifted significantly to a more alkaline value of 6.86 ± 0.05 ($p = 0.0082$; Fig. 11C).

To assess the effect of T3 on desensitization, SSD curves were obtained by pre-applying conditioning pH values from pH 7.6 to 6.3, followed by activation with fully activating pH 6.0 (Fig. 11B). Under control conditions, the pH_{50} of SSD was 7.03 ± 0.02, whereas in the presence of T3 it was slightly but significantly shifted to 7.08 ± 0.01 ($p = 0.0324$; Fig. 11C), indicating that T3 increased the proton sensitivity of rASIC3 for both activation and steady-state desensitization. Notably, the activation curve exhibited a larger alkaline shift than the SSD curve, thereby expanding the overlap between them, leading to an increased window current.

To more directly evaluate T3's effect on the window current, we gradually lowered the pH from 7.3 to 6.8 in 0.1-unit steps (Fig. 11D). As expected, in the absence of T3, a small window current was observed, peaking at pH 7.0. However, in the presence of 5 μM T3, the window current was strongly enhanced across the pH range of 7.2 - 6.8, with the greatest potentiation occurring at pH 7.1 (Fig. 11E)

Taken together, these results show that, similar to its effects on rASIC1a, T3 potentiated rASIC3 currents at micromolar concentrations. However, unlike for rASIC1a where T3 likely increases proton efficacy, for rASIC3, T3 enhances proton sensitivity. Furthermore, both types of sustained currents, window currents at near-neutral pH and sustained currents under very acidic conditions, were potentiated by T3.

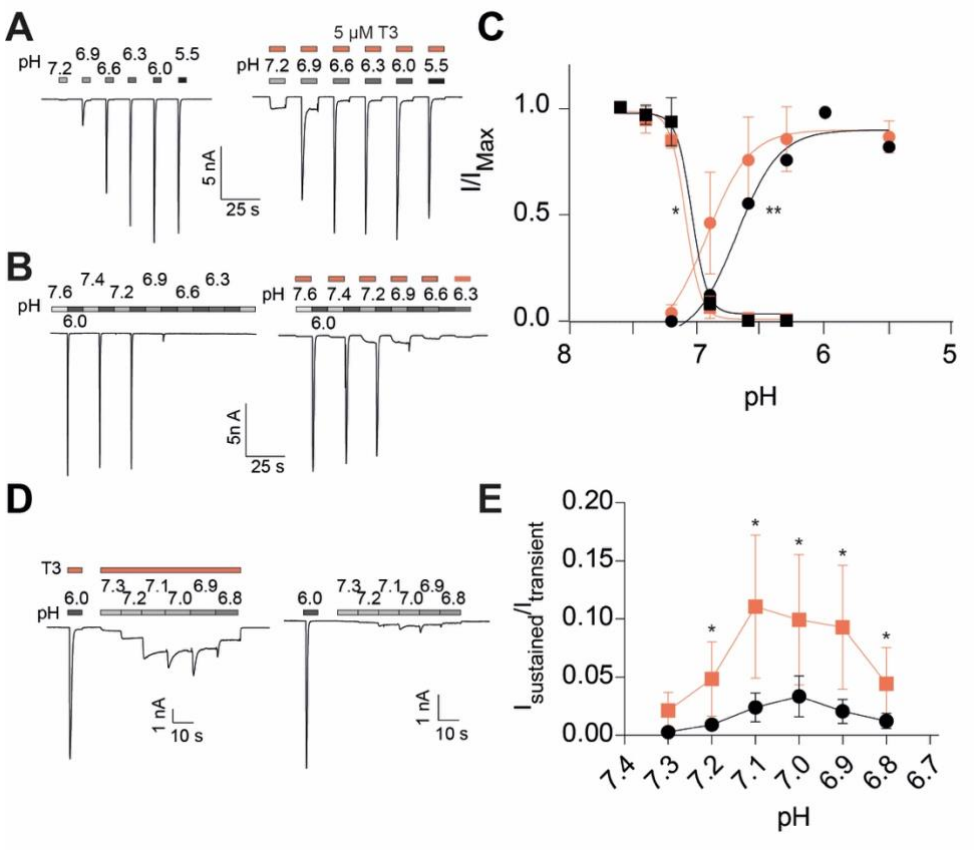

Figure 11. The thyroid hormone T3 increases rASIC3 window currents. (A) Representative current traces from HEK 293 cells expressing rASIC3. ASIC3 was repeatedly activated by different pH in the absence (left) or presence (right) of 5 µM T3. **(B)** rASIC3 was activated by pH 6.0 with varying pre-conditioning pH in the absence (left) or presence (right) of 5 µM T3. **(C)** pH-response curves for activation (circles) and steady-state desensitization (squares) in the absence (black) or presence of T3 (red). Lines represent fits to the Hill equation (n = 8). **(D)** rASIC3 was once fully activated by pH 6 and subsequently pH was gradually increased from pH 7.3 to pH 6.8 in the presence or absence of 5 µM T3. **(E)** Quantitative analysis of rASIC3 window currents between pH 7.3 and pH 6.8. Currents were normalized to the peak current at pH 6.0 (n = 7). Bars represent mean ± SEM. *, $P < 0.05$; **, $P < 0.01$.

3.3. Effect of T3 on human ASICs

3.3.1. The human thyroid cell line Nthy-ori-3-1 expresses functional ASICs, which are not potentiated by T3

So far, our data indicate that T3 potentiates rASIC1a and rASIC3 currents at micromolar concentrations. However, in physiological conditions, total plasma T3 is typically in the nanomolar range, and free T3 concentrations are even lower, within the picomolar range [69]. We speculated that T3 released from thyroid follicular cells could reach local concentrations sufficient to affect ASICs.

To investigate the possibility that thyroid follicular cells express functional ASICs, we used the Nthy-ori-3-1 cell line, an immortalized normal human thyroid follicular epithelial cell line (a kind gift from Prof. Paola Caria; Table 15), as a model to study endogenous ASIC expression and function in the thyroid.

To assess ASIC expression, first, qPCR for *Asic1*, *Asic2*, *Asic3*, and *Asic4* was performed by my colleague Jingyu Yang. She found that Nthy-ori-3-1 cells primarily express *Asic1* and to a lesser extent *Asic3*, while *Asic2* and *Asic4* expression were not detected (Fig. 12A, left). This expression pattern is generally consistent with publicly available datasets fur human thyroid tissue (e.g., GEPIA2 [95]), although the database reports higher expression of *Asic3* relative to *Asic1*, and also lacks detectable expression of *Asic2* and *Asic4* (Fig. 12A, right).

To study endogenous ASICs in Nthy-ori-3-1 cells in more detail, we applied different extracellular pH values (7.0, 6.5, and 6.0). Since the exact ASIC subtype and their electrophysiological properties was unknown, we selected pH 6.0 to broadly activate ASICs, pH 7.0 to activate window current, and pH 6.5 to estimate the pH_{50} by comparison the response amplitude to that at pH 6.0. We found that pH 6.0 elicited a transient inward current with ASIC-like properties, while pH 6.5 evoked a transient current of roughly half the amplitude, suggesting a pH_{50} close to pH 6.5. At pH 7.0, a small, sustained current was observed (Fig. 12B). These data indicate that extracellular acidification activated transient inward currents in Nthy-ori-3-1 cells, consistent with the presence of functional ASICs.

Surprisingly, the application of 5 µM T3 did not enhance ASIC currents neither at pH 7.0 nor at pH 6.5 and failed to induce any response at pH 7.4 (Fig. 12B). Even when the T3 concentration was increased to 10 or 20 µM, no significant potentiation was observed at pH 6.5

(P = 0.077 for 20 µM T3; Fig. 12C), suggesting that endogenous ASICs in Nthy-ori-3-1 cells are not significantly modulated by T3.

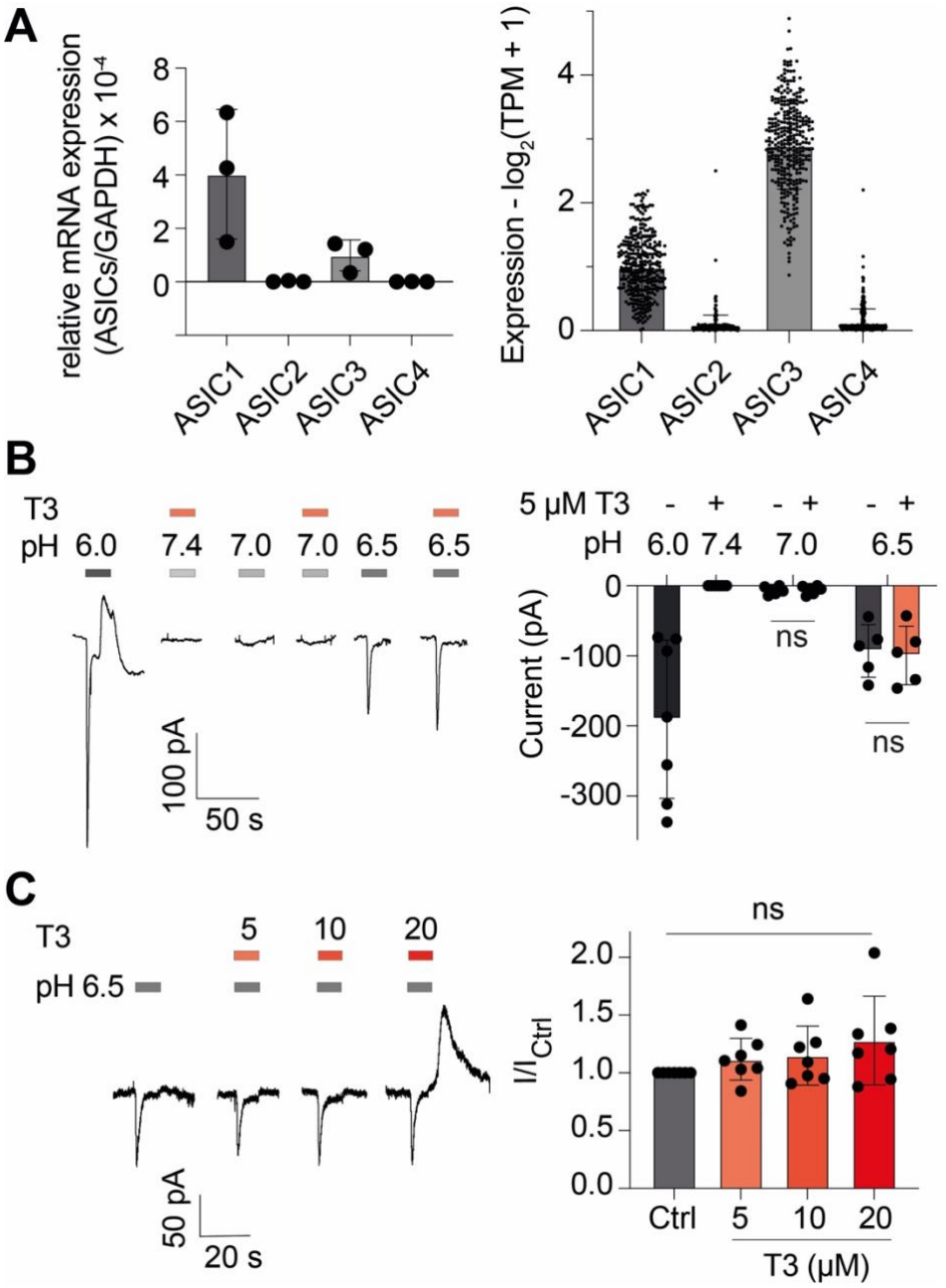

Figure 12. The thyroid hormone T3 does not potentiate ASIC-like currents in the human thyroid gland cell line Nthy-ori-3-1. (A) Left, RNA expression of *Asic1*, *Asic2*, *Asic3*, and *Asic4* in Nthy-ori-3-1 cells, normalized to the expression of *GAPDH*. Dots represent biological replicates, n = 3 for every condition, with three technical replicates for each biological replicate (this experiment performed by Ms. Jingyu Yang). Right, Expression profiles of *Asic1*, *Asic2*, *Asic3*, and *Asic4* in thyroid gland based on the GEPIA2 database **(B)** Left, representative current trace of an Nthy-ori-3-1 cell, exposed to different proton concentrations (pH 7.0, pH 6.0 and pH 6.5) in the absence or presence of 5 µM T3. Right, quantitative analysis of peak inward currents (n = 5). **(C)** Left, representative current trace of an Nthy-ori-3-1 cells, exposed to pH 6.5 in the presence of different T3 concentrations (5, 10, and 20 µM). Right**,** quantitative analysis of peak inward currents (n = 7). Bars represent mean ± SEM. ns, not significant.

3.3.2. T3 sensitivity of human ASIC1a, ASIC3, and ASIC1a/3 heteromers

Since T3 failed to potentiate ASIC currents in the human Nthy-ori-3-1 thyroid cell line, we considered that T3 is unable to potentiate certain human ASIC (hASIC) subtypes. Given that Nthy-ori-3-1 cells predominantly express *Asic1* and *Asic3*, the dominant endogenous ASIC channel in this cell line could be composed of hASIC1 homomers, hASIC3 homomers, or hASIC1a/3 heteromers.

To explore whether the subunit composition affects T3 sensitivity, we expressed homomeric hASIC1, homomeric hASIC3, and heteromeric hASIC1/3 in *Xenopus* oocytes and evaluated their responses to T3. The oocytes expression system was chosen due to its suitability for expressing heterometric ASICs.

For hASIC1a homomers, we applied pH 6.0 and pH 6.5 in the presence and absence of 5 µM T3, to determine whether T3 potentiates currents during maximal and half-maximal activation. In the absence of T3, hASIC1 was activated by pH 6.5 and exhibited desensitization with a time constant (τ) of 2.76 ± 0.44 s. Co-application of 5 µM T3 strongly potentiated hASIC1a-mediated currents by approximately twofold at pH 6.5 ($P = 0.08$), but had no effect at pH 6.0. Thus, T3 potentiated hASIC1a similar to rASIC1a (Fig. 14A).

In contrast, hASIC3 homomer-expressing oocytes displayed a distinct T3 response. Unexpectedly, at pH 7.4, application of 1 µM T3 induced a large sustained inward current. At pH 6.0, near the pH_{50} for hASIC3, T3 did not potentiate the transient current amplitude. Instead, it induced a large sustained current that followed the proton-evoked transient activation, indicating a unique, possibly noncanonical activation of hASIC3 by T3 (Fig. 14B). This action will be further characterized below. Notably, despite using the same amounts of RNA for injection, hASIC3 generated significantly smaller proton-induced current amplitudes compared to hASIC1 (0.51 ± 0.09 µA for hASIC3 vs. 22.54 ± 7.25 µA for hASIC1).

In oocytes co-expressing hASIC1a and hASIC3 (RNA ratio hASIC1a: hASIC3 = 1:30), currents desensitized more rapidly (τ = 0.67 ± 0.25 s), and T3 potentiation at pH 6.5 was weak (1.35-fold, $P = 0.399$), with no potentiation observed at pH 6.0 (Fig. 14C). This pattern closely resembled the T3 insensitivity of ASICs seen in thyroid epithelial cells.

Given that ASIC currents in Nthy-ori-3-1 cells also showed fast desensitization (τ = 1.09 ± 0.03 s at pH 6.5), comparable to heteromeric ASIC1a/3 (Fig. 13; $P = 0.93$ for a 1:10 ratio, $P = 0.44$

for 1:20, and $P = 0.13$ for 1:30), and that T3 neither potentiated transient ASIC currents nor induced sustained activity at neutral pH, it is unlikely that the dominant ASIC in these cells is a hASIC1a or hASIC3 homomer. Instead, these properties point toward heteromeric hASIC1a/3 channels being the major functional ASIC subtype in Nthy-ori-3-1 cells.

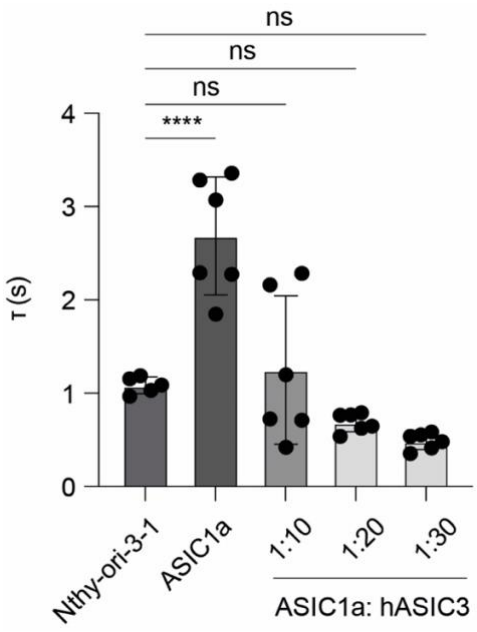

Figure 13. Desensitization time constant (τ) of ASIC currents. Currents were recorded in Nthy-ori-3-1 cells, in *Xenopus* oocytes expressing homomeric hASIC1a, or in oocytes expressing heteromeric hASIC1/3 channels at varying injection ratios of hASIC1a to hASIC3 RNA. ns, not significant; ****, $P < 0.0001$.

To further characterize hASIC1a/3 heteromers, we recorded both activation and steady-state desensitization (SSD) curves in the presence or absence of T3. These experiments were performed in a manner similar to those shown in Fig. 11A and 11B. In the absence of T3, hASIC1/3-mediated currents saturated at pH 6.0 and had a pH_{50} of 6.48 ± 0.08. In the presence of T3, the activation curve was slightly but not significantly shifted to the left (pH_{50} = 6.61 ± 0.06, $P = 0.0695$, Fig. 14D). Similarly, T3 caused a slight but not significant right-shift of the SSD curve (without T3, pH_{50} = 7.19 ± 0.02; with T3, pH_{50} = 7.13 ± 0.03; $P = 0.118$; Fig. 14D).

Taken together, these results indicate that if T3 has any modulatory effects on hASIC1a/3 heteromers, these are subtle. Given that T3 failed to potentiate ASIC currents in Nthy-ori-3-1 cells and that the desensitization kinetics (τ_{des}) of ASICs in these cells more closely resembled those of hASIC1a/3 than of homomeric hASIC1a, we conclude that the predominant ASIC subtype in Nthy-ori-3-1 cells is likely heteromeric hASIC1a/3. This subunit composition would explain the lack of potentiation or direct activation by T3 in this human thyroid epithelial cell line.

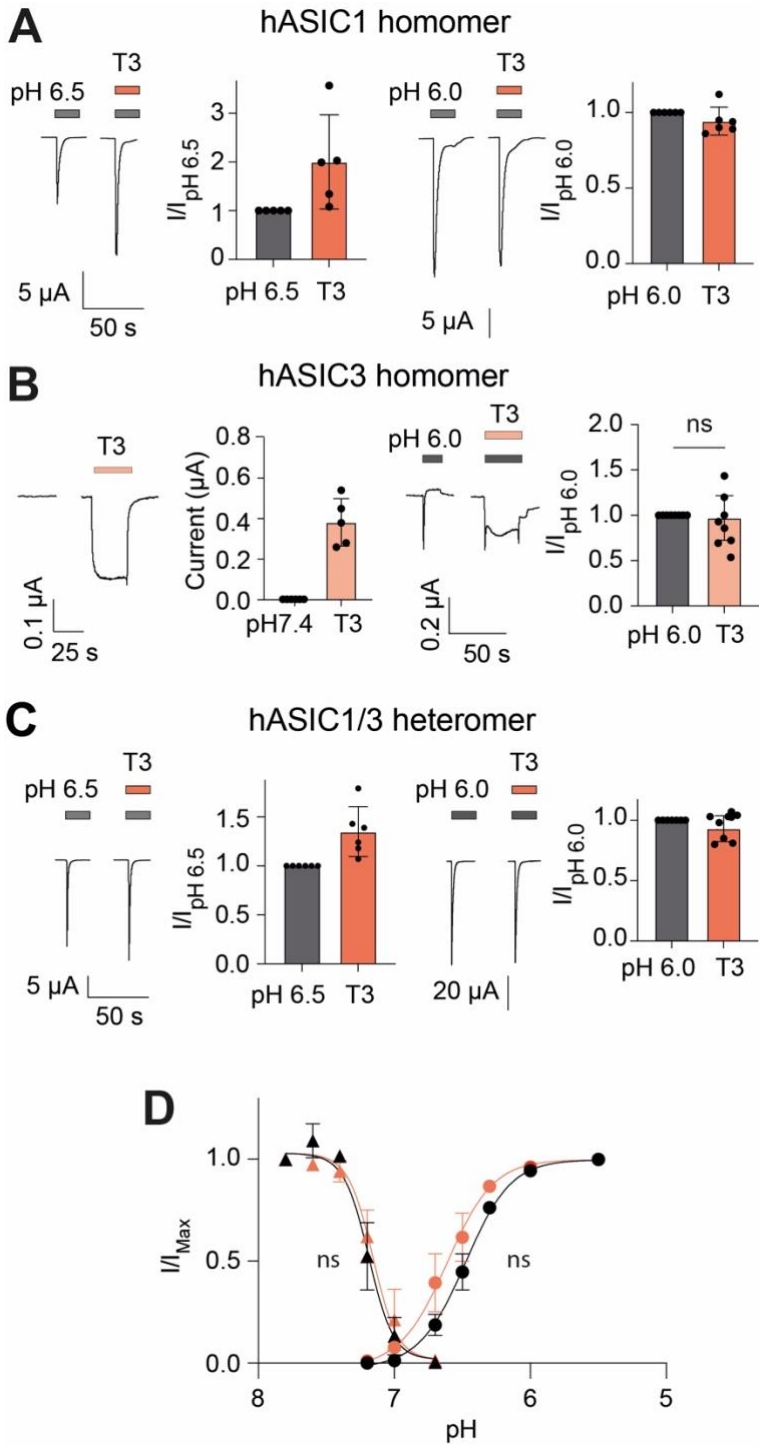

Figure 14. Effect of thyroid hormone T3 on human ASIC1, ASIC3 and heteromeric ASIC1a/3 expressed in *Xenopus* oocytes. (A) Left, representative current traces of hASIC1a. Currents were elicited by pH 6.5 or pH 6.0 in the absence or presence of 5 µM T3. Right**,** quantitative analysis of peak currents. **(B)** Left, representative current traces of hASIC3. Currents were elicited by T3 at pH 7.4 or pH 6.0. Right, quantitative analysis of sustained and peak currents in the presence or absence of 1 µM T3. **(C)** Left, representative current traces of heteromomeric hASIC1a/3, activated by pH 6.5 or pH 6.0 in the absence or presence of 5 µM T3. Right, quantitative analysis of peak currents. **(D)** pH-response curves for activation (circles) and steady-state desensitization (squares) in the absence (black) or presence (red) of 5 µM T3. Lines represent fits to the Hill equation (n = 8). Bars represent mean ± SEM. ns, not significant.

3.3.3. T3 strongly activates human ASIC3 with micromolar apparent affinity

In the previous experiments, we found that T3 did not potentiate the transient current of hASIC3. Instead, it induced a large, sustained current at neutral pH. To investigate this effect in more detail, we expressed hASIC3 in oocytes and activated it maximally with pH 5.5, and applied various concentrations of T3, ranging from 10 nM to 20 µM, at pH 7.4.

In the absence of T3, pH 5.5 elicited a small transient inward current, followed by an outward current, consistent with previously reported findings. Remarkably, T3 induced large sustained inward currents at neutral pH. This response was absent in non-injected oocytes and in oocytes expressing ASIC1a, indicating an effect specific to hASIC3. The amplitude of the T3-induced sustained current increased with increasing T3 concentrations and did not saturate at concentrations up to 20 µM (estimated EC_{50} > 100 µM; Fig. 15A).

Strikingly, at concentrations > 1 µM, the T3-induced current exceeded the amplitude of the proton-evoked response at pH 5.5. At 20 µM T3, the current was approximately 60 times greater than the current evoked by pH 5.5, indicating that T3 is far more efficient than protons to activate hASIC3. Notably, even nanomolar concentrations of T3 (10 -100 nM) were sufficient to evoke small sustained currents in hASIC3-expressing oocytes (Fig. 15A). At approximately 1 µM T3, the amplitude of the sustained current was comparable to that of the hASIC3 current elicited by pH 5.5 (P = 0.612; 15B).

Taken together, T3 exhibits a unique ability to induce a large sustained hASIC3 current at neutral pH, a phenomenon not observed with other ASIC subunits, indicating a distinct modulatory mechanism specific to hASIC3.

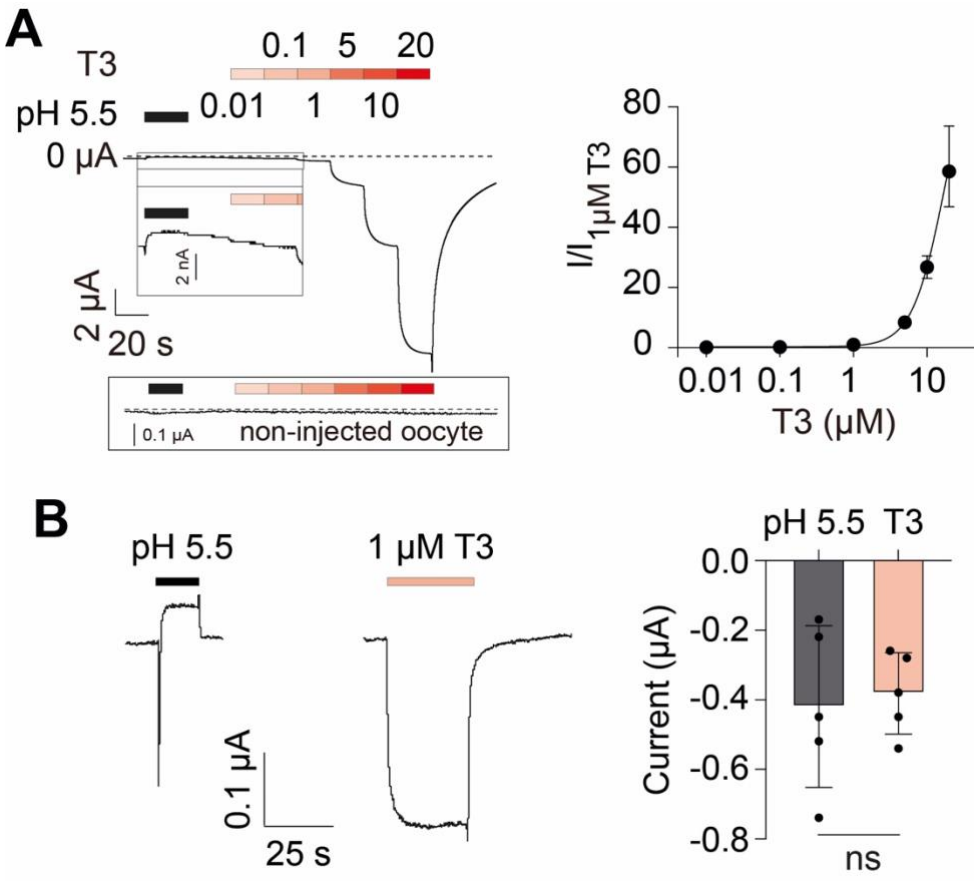

Figure 15. The thyroid hormone T3 activates hASIC3 independent of protons. (A) Left, representative current trace of a hASIC3-expressing oocyte. hASIC3 was activated by increasing concentrations of T3 at pH 7.4. The insert shows the activation by pH 5.5 and by nanomolar concentrations of T3. Right, concentration-response curve. The line represents a fit to the Hill equation. **(B)** Left, representative current traces of hASIC3b, activated by pH 5.5 and subsequently by 1 µM T3. Right, quantitative analysis of transient proton-activated and of sustained T3-activated currents; n = 5. ns, not significant.

3.3.4. T3 elicits amiloride-sensitive Na^+ currents in cells expressing human ASIC3

To further characterize the activation of hASIC3 by T3, a series of experiments were conducted.

First, we examined whether the sustained current induced by T3 is specific to T3 or shared with other thyroid hormones. To this end, we applied 5 μM T3, T2, or T4 to hASIC3-expressing oocytes. Despite their structural similarities, T2 failed to elicit sustained currents at neutral pH, and T4 induced much smaller currents than T3 (Fig. 16A). These results suggest that specific molecular features of T3 are essential for its ability to efficiently activate hASIC3.

As further evidence of proton-independent activation, we applied 5 μM T3 at various pH values. Notably, T3 induced robust sustained currents even at alkaline pH (pH 8.0), with amplitudes comparable to those at pH 7.4 ($P > 0.99$). In contrast, the amplitude of T3-induced currents progressively decreased as the pH became more acidic ($P = 0.0064$ vs. pH 6.5, $P = 0.002$ vs. pH 6.0; Fig. 16B), reinforcing the idea that T3 can activate hASIC3 independently of protons.

To determine whether the T3-induced current exhibited typical ASIC properties, we tested its sensitivity to amiloride, a well-known ASIC pore blocker. T3-induced currents decreased in a concentration-dependent manner upon co-application of amiloride and were almost completely blocked at millimolar concentrations ($IC_{50} = 240 \pm 16$ μM; Fig. 16C). Interestingly, 10 μM amiloride transiently potentiated the T3-induced current, consistent with previously reported biphasic effects of amiloride on rASIC3 [52]. This phenomenon may be attributed to the existence of two distinct amiloride-binding sites.

To assess the ion selectivity of the T3-induced current, we measured the reversal potential (E_{rev}) using a ramp protocol from -70 to +50 mV in the presence of 5 μM T3. For comparison, proton-induced currents were recorded at pH 5.5 under varying holding potentials. The reversal potential of proton-evoked currents was +45.4 ± 4.4 mV, while that of T3-induced currents was +36.5 ± 5.5 mV (Fig. 16D; $P = 0.24$), suggesting that T3-induced currents are also Na^+-selective. The slightly less positive E_{rev} may indicate a lower selectivity but could also be due to a changed Na^+ equilibrium potential due to the sustained Na^+ influx during T3 activation of hASIC3.

Taken together, these results demonstrate that T3 specifically and directly activated hASIC3 homomers in a proton-independent manner, inducing robust sustained currents even under neutral or alkaline conditions. This effect was not observed with other thyroid hormones, was

sensitive to amiloride inhibition, and was Na^+-selective, indicating that T3 may serve as a distinct endogenous ligand for hASIC3.

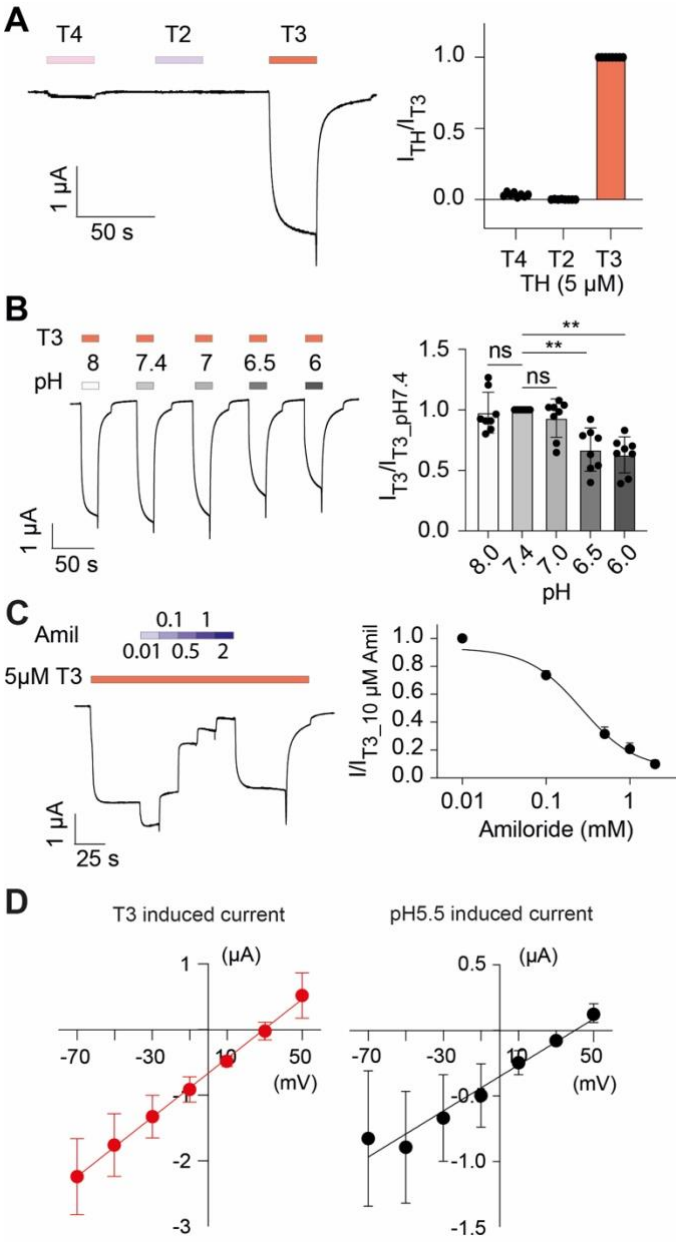

Figure 16. Characterization of T3-induced sustained currents in *Xenopus* oocytes (A) Left, representative current trace of hASIC3, elicited by 5 µM T2, T4, or T3. Right, quantitative analysis of sustained current amplitudes (n = 8). **(B)** Left, representative current trace of hASIC3, elicited by 5 µM T3 at different proton concentrations. Right, quantitative analysis of T3-induced currents. **(C)** Left, representative current trace of hASIC3, elicited by 5 µM T3 and inhibited by increasing concentrations of amiloride. Right, mean concentration-response curve for amiloride. The curve represents a fit to the Hill equation. **(D)** Current-voltage relationships of hASIC3, activated by 5 µM T3 (left) or pH 5.5 (right). T3-induced currents were recorded at continuously increasing holding potentials from −70 to +50 mV within 1 s. pH 5.5-induced currents were recorded by stepwise increases in the holding potential from -70 to +50 mV. Dots represent the mean and bars the SEM (n = 5). ns, not significant; **, $P < 0.01$.

3.4. T3 induced outward current in Nthy-ori-3-1 cell line

In the previous experiments, we demonstrated that T3 can potentiate or activate various ASIC subtypes. In contrast, T3 failed to modulate endogenous ASICs in a thyroid epithelial cell line. However, unexpectedly, in these cells, at pH 6.5 20 µM T3 elicited a large outward current (Fig. 12C). To investigate this outward current in more detail, we conducted a series of electrophysiological recordings aimed at addressing the following key questions:

1. Which extracellular stimulus triggers the outward current?

2. Which conductance underlies this outward current?

3. What is the underlying mechanism of its induction?

3.4.1. Which extracellular stimulus triggers the outward current in Nthy-ori-3-1 cells?

As the outward current was observed at pH 6.5 and 20 µM T3, both thyroid hormone T3 and extracellular acidic pH are potential contributors to the induction of the outward current (see, for example, Fig. 12C). To investigate whether T3 and acidic pH activated the outward current independently, synergistically or cooperatively, we applied varying concentrations of T3 (from 1 µM to 10 µM) at pH 6.0. As previously observed, the outward current appeared when both T3 and acidic pH were present. Upon stimulation, the outward current rapidly increased to a peak within 10 seconds, followed by a gradual decline. During washout of T3 and low pH, the current transiently increased before quickly returning to baseline or even below baseline, indicating that the outward current was quickly reversible (Fig. 17A). Moreover, the amplitude of the outward current increased with increasing T3 concentrations.

Interestingly, while the induction of the outward current required 20 µM T3 at pH 6.5 (as shown in Fig. 12C), 5 µM T3 was sufficient to induce an outward current at the more acidic pH 6.0. This observation suggests that stronger acidity reduces the concentration threshold of T3 required to elicit the outward current, or potentially, that very acidic conditions alone are sufficient. To test this hypothesis, we applied an extracellular solution of pH 5.0 without T3. pH 5.0 alone was indeed sufficient to evoke an outward current. In contrast, no such current was observed at pH 6.0 or 6.5 in the absence of T3 (Fig. 17B), indicating that the current is pH-sensitive and that its pH-sensitivity is increased by T3.

Furthermore, although application of 10 μM T3 at pH 5.0 did not significantly enhance the amplitude of the outward current, it significantly shortened the onset of activation (from 12.3 s to 4.6 s, $P = 0.0003$, Fig. 17C), the interval between stimulus and peak current, suggesting that T3 accelerated the activation of the acid-induced outward current even at acidic pH.

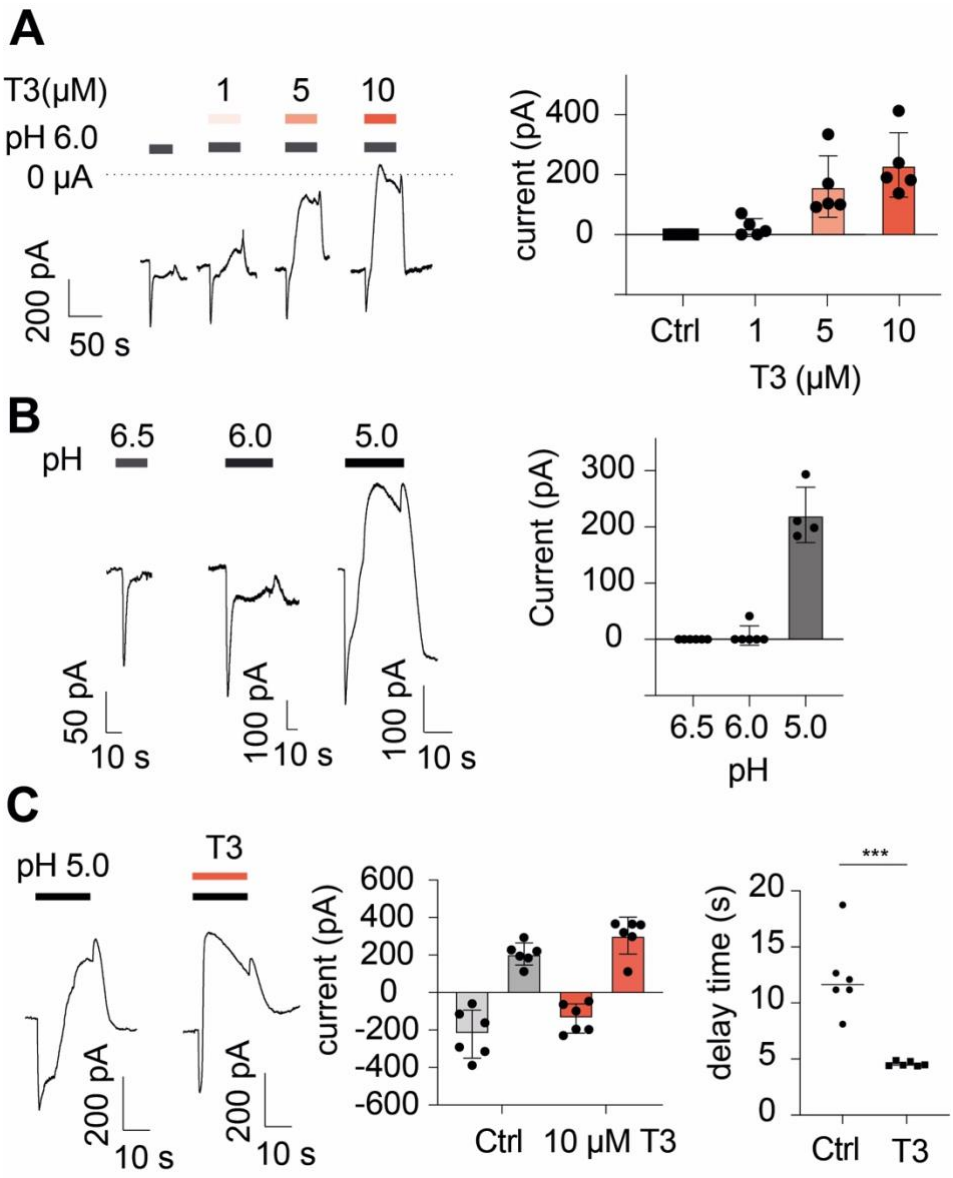

Figure 17. Extracellular acidification induces an outward current that is modulated by T3 in Nthy-ori-3-1 cells. (A) Left, representative current traces from Nthy-ori-3-1 cells exposed to pH 6.0 with co-application of increasing concentrations of T3 (1, 5, and 10 μM). Right, quantification of peak outward currents in the absence or presence of different concentrations of T3. **(B)** Left, representative current traces in response to pH 6.5, pH 6.0, or pH 5.0 in the absence of T3. Right, quantitative analysis of peak outward currents at the indicated pH values. **(C)** Left, Representative current traces evoked by pH 5.0 in the absence or presence of 10 μM T3. Middle, quantification of peak inward and outward currents. Right, analysis of delay time (from stimulus application to peak current) in the absence or presence of T3. Dots represent individual data points; bars indicate mean ± SEM (n = 6). ***, $P < 0.001$.

3.4.2. Which conductance underlies the outward current – ion selectivity?

In the previous section, we demonstrated that the outward current is induced by acidic pH and modulated by T3.

According to the Nernst equation, the reversal potentials for Na^+, Cl^-, and Ca^{2+} in these experiments were approximately +65 mV, -30 mV, and +131 mV (Tab. 16), respectively, each substantially more positive than -70 mV, the holding potential throughout the recordings. In contrast, the K^+ reversal potential was around -90 mV (Tab. 16), which is more negative than the holding potential. Thus, the outward current was either mediated by activation of a K^+ or Cl^- conductance or by inhibition of a Na^+ or Ca^{2+} conductance.

To assess whether the outward current was carried by K^+, we employed an extracellular solution with elevated concentration $[K^+]_e$ (Tab. 11), which shifts the K^+ reversal potential from -90 mV to approximately -70 mV, equal to the holding potential. We will refer to this solution as the "Erev(K) solution."

As shown previously, 10 µM T3 at pH 6.0 reliably induced an outward current under standard conditions. However, when the Erev(K) solution was perfused, the outward current was abolished. Upon switching back to normal Ringer's solution, the current reappeared (Fig. 18A). Similarly, when the experiment was started in Erev(K) solution, no outward current was observed until the bath was exchanged for standard solution (Fig. 18B).

Ion	$[Ion]_e$ (mM)	$[Ion]_i$ (mM)	z	E_{rev} (mV)
K^+	3.6	125	1	-90.53
Na^+	140	10.8	1	65.38
Ca^{2+}	3	0.0001	2	131.64
Cl^-	117	34.7	-1	-30.97

Table 16. Reversal potentials according to the Nernst equation.

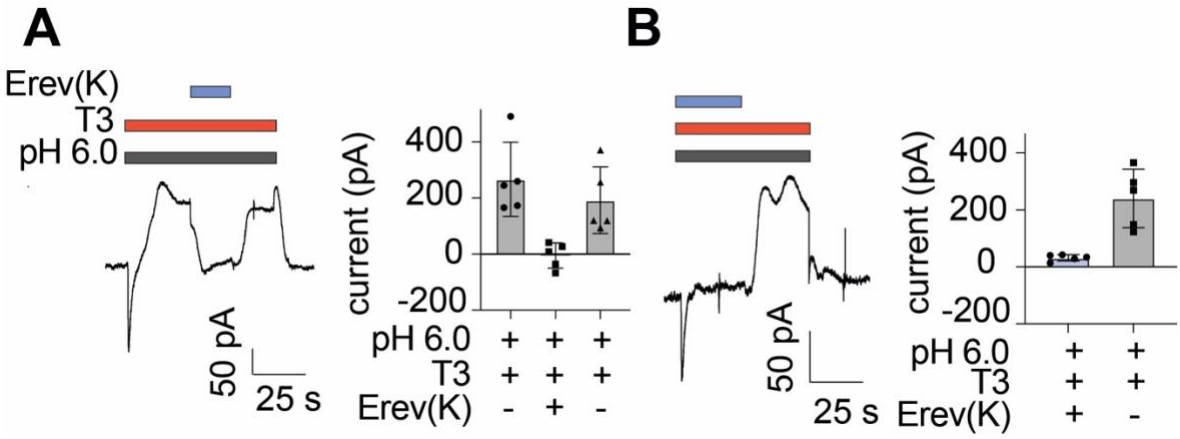

Figure 18. The outward current is carried by K^+ ions. (A) Left, representative current traces from Nthy-ori-3-1 cells exposed to pH 6.0 together with 10 µM T3. During activation, the extracellular solution was exchanged with the Erev(K) solution containing the same T3 concentration and pH. Right, quantification of peak outward currents recorded in normal Ringer's solution before and after the Erev(K) solution compared with the Erev(K) solution. **(B)** Left, representative current traces from Nthy-ori-3-1 cells exposed to pH 6.0 and 10 µM T3, with the Erev(K) solution present from the beginning of the activation. Right, quantification of peak outward currents in normal Ringer's solution and Erev(K) solution. Bars indicate mean ± SEM (n = 6). *, $P < 0.05$; **, $P < 0.01$.

3.4.3. What is the mechanism underlying the induction of the outward current?

To this point, we have demonstrated that the outward current is a K^+ current, is activated by acidic extracellular pH and modulated by T3. The next question we addressed was the underlying mechanism of its induction.

Given that the delay time to peak outward current (as shown in Fig. 17C) was approximately 12 seconds at pH 5.0 and was shortened in the presence of T3, it is unlikely that the current arises from direct proton activation of a K^+ channel. Direct channel activation typically occurs on the millisecond scale and would not be significantly accelerated by T3. On this basis, the following ion channels were considered:

1. Na^+-activated K^+ channels, secondarily activated by ASIC activation
2. Ca^{2+}-activated K^+ channels

To test the first hypothesis, we replaced extracellular Na^+ by NMDG using a modified Ringer solution (see Tab. 10). When 10 µM T3 and pH 6.0 were applied under these Na^+-free conditions, the outward current was still evoked (Fig. 19A), indicating that Na^+ was not required for its activation. Interestingly, after switching to NMDG solution the baseline current was reduced, suggesting the presence of a persistent Na^+ leakage current in Nthy-ori-3-1 cells. Furthermore, the outward current decayed more rapidly under Na^+-free conditions.

To determine whether the outward current depended on ASICs, we applied 100 µM amiloride to block ASIC currents. As shown in Fig. 19B, even though ASIC-mediated currents were almost completely abolished, the outward current was still present and not significantly reduced compared with control conditions. This indicates that the outward current was not dependent on ASIC activation and further rules out the involvement of Na^+-activated K^+ channels.

To evaluate whether Ca^{2+} influx was responsible, we used an extracellular Ca^{2+}-free solution (Tab. 9). The outward current induced by 10 µM T3 at pH 6.0 remained unchanged under Ca^{2+}-free conditions (Fig. 19C), suggesting that extracellular Ca^{2+} was not required. Interestingly, switching from normal to Ca^{2+}-free solution increased the baseline current, implying that extracellular Ca^{2+} modulated the leak current.

Finally, to test whether intracellular Ca^{2+} might play a role, we applied 5 µM ionomycin, a Ca^{2+} ionophore known to increase intracellular Ca^{2+} by promoting both influx and release from internal stores. Under these conditions, a robust outward current was induced (Fig. 19D). When

the bath solution was switched to the Erev(K) solution (with elevated K^+ to nullify the driving force), the outward current was abolished, confirming that it was carried by K^+ ions.

Taken together, the outward current was not inhibited by Na^+-free (NMDG) or Ca^{2+}-free solutions and persisted in the presence of the ASIC blocker amiloride. However, it was robustly induced by ionomycin. These findings indicate that the current was not mediated by ASIC activation or Na^+-activated K^+ channels. Instead, it was most likely mediated by Ca^{2+}-activated K^+ channels, with intracellular Ca^{2+} acting as the key activator.

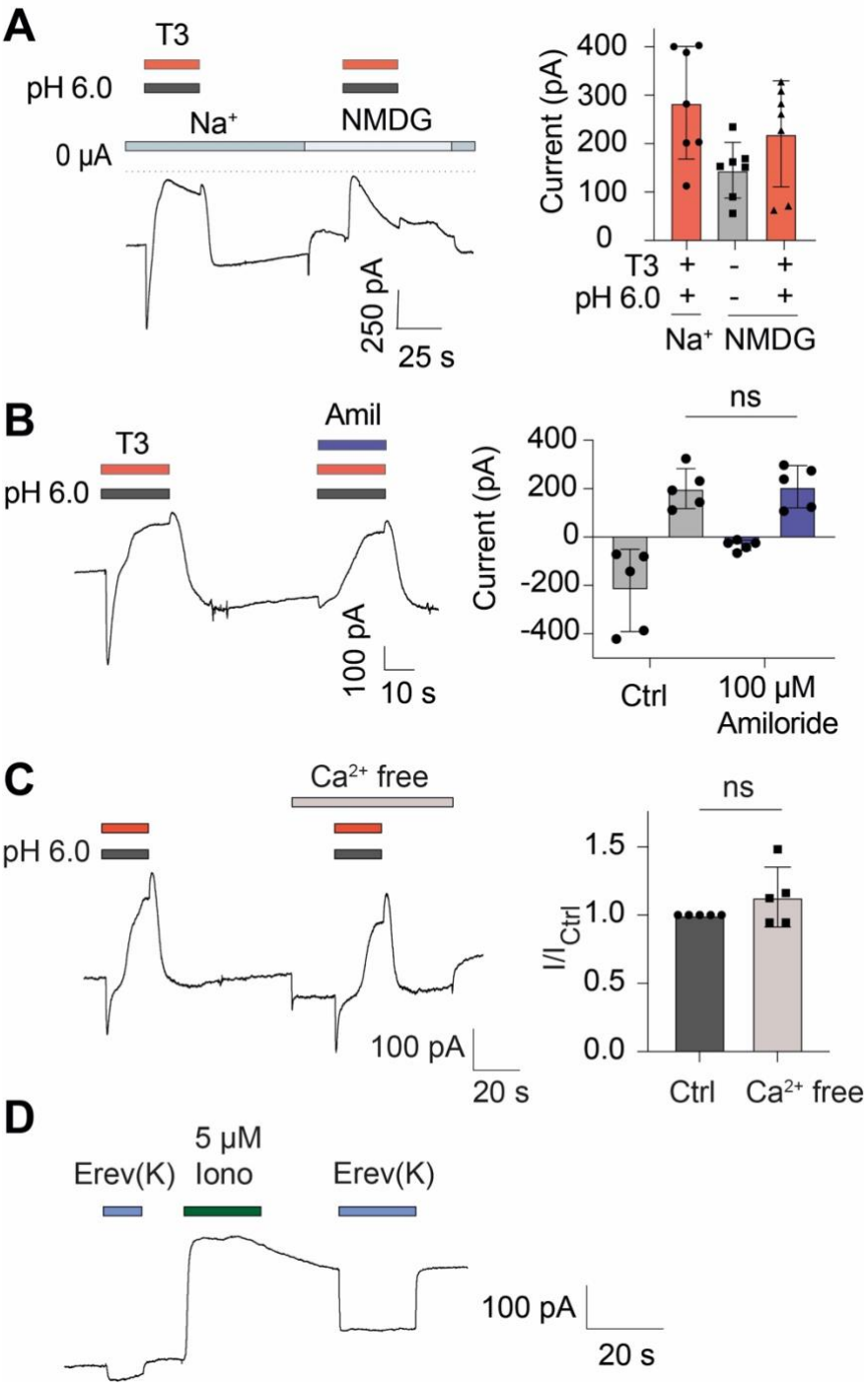

Figure 19. Outward current is induced by increased intracellular Ca^{2+} concentration. (A) Left, representative current traces from Nthy-ori-3-1 cells exposed to pH 6.0 with co-application of 10 µM T3 in normal Ringer's solution and in NMDG-based solution. Right, quantification of peak outward currents (n = 7). **(B)** Left, representative currents evoked by 10 µM T3 at pH 6.0 in the presence and absence of 100 µM amiloride. Right, quantification of peak outward currents (n = 5). **(C)** Left, representative currents evoked by 10 µM T3 at pH 6.0 in normal versus Ca^{2+}-free Ringer's solution. Right, quantification of peak outward currents (n = 5). **(D)** Trace representative for 4 similar measurements illustrating the outward current evoked by 5 µM ionomycin in normal and Erev(K) solution (n = 4). Bars represent mean ± SEM. ns, not significant; *, $P < 0.05$.

3.4.4. Ca^{2+} Imaging of pH and T3 Effects in Thyroid Cells

To examine in more detail how acidic pH and T3 modulated intracellular Ca^{2+} responses, we performed Ca^{2+} imaging experiments under various pH conditions, with and without T3. In these experiments, Fura-2 was used as a Ca^{2+}-sensitive fluorescent indicator, and 5 μM ionomycin served as a positive control to validate the system.

As shown in Figure 20A, extracellular acidification to pH 6.0 elicited a significant increase in intracellular Ca^{2+} concentration $[Ca^{2+}]_i$ ($P = 0.0032$ vs. baseline), and this effect was even more pronounced at pH 5.0, indicating a pH-dependent increase in $[Ca^{2+}]_i$. Interestingly, when 10 μM T3 was applied alone at neutral pH 7.4, it triggered a small but statistically significant increase in $[Ca^{2+}]_i$ ($P = 0.0082$ vs. baseline). When T3 was co-applied with pH 6.0, the Ca^{2+} signal was substantially enhanced ($P = 0.0003$ vs. 10μM T3). A direct comparison of Ca^{2+} responses to pH 6.0 in the absence and presence of T3 revealed a significant potentiation by T3, consistent with the patch-clamp results described earlier.

A $[Ca^{2+}]_i$ increase can arise via several pathways, among which G-protein-coupled receptors (GPCRs), particularly those signaling through Gq proteins, are well known to activate phospholipase C and induce Ca^{2+} release via IP_3-mediated pathways. To investigate whether a GPCR pathway was involved, we applied YM-254890, a broad-spectrum G-protein inhibitor with selectivity for Gq and Gs pathways [96, 97]. YM-254890 was applied for 30 minutes prior to Ca^{2+} imaging and was co-applied with the stimuli during Ca^{2+} imaging. As shown in Fig. 20B, in the presence of YM-254890, stimulation with pH 5.0 or 10 μM T3 plus pH 6.0 no longer elicited any significant $[Ca^{2+}]_i$ increase; in fact, a reduction in basal $[Ca^{2+}]_i$ was observed (Fig. 20B, left). These results suggest that the Ca^{2+} response was mediated by proton-sensitive GPCRs.

Consistent with the Ca^{2+} imaging data, pre-treatment with YM-254890 for 30 minutes also abolished the T3- and pH-induced outward current in patch-clamp recordings (Fig. 20C, right), further supporting the conclusion that the outward K^+ current was dependent on intracellular Ca^{2+} and was mediated by a GPCR signaling cascade activated by protons.

Taken together, the outward current observed in Nthy-ori-3-1 cells was mediated by Ca^{2+}-activated K^+ channels, which were secondarily activated by a proton-sensitive GPCR. This GPCR appears to be directly activated by extracellular protons, whereas T3 modulated its activation and, to a lesser extent, weakly activated the receptor directly.

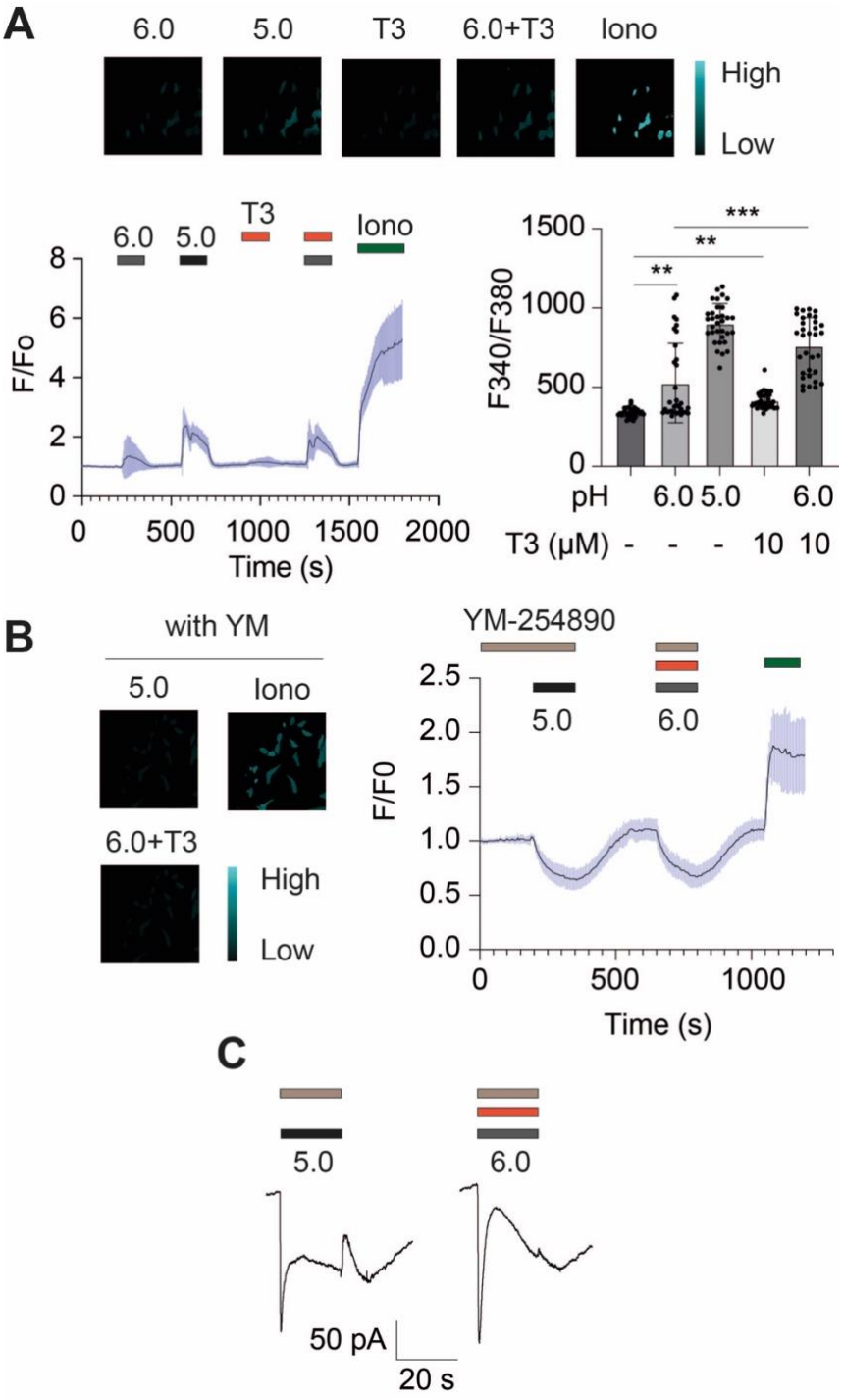

Figure 20. Ca^{2+} imaging reveals intracellular Ca^{2+} responses evoked by extracellular acidification and T3 in Nthy-ori-3-1cells. (A) upper, representative images of Ca^{2+}-imaging experiments. Down right, mean ± SD of all Ca^{2+}-imaging experiments of Nthy-ori-3-1 cells stimulated with pH 6.0, pH 5.0, 10 μM T3, pH 6.0+10 μM T3, 5 μM ionomycin was used as a positive control (n = 36). Down right, quantification of peak Ca^{2+} responses. **(B)** Left, representative images of Ca^{2+}-imaging experiments. Right, mean ± SD of all Ca^{2+}-imaging experiments of Nthy-ori-3-1 cells in response to pH 5.0 or pH 6.0+10 μM T3 in the presence of 1 μM YM-254890. YM-254890 was pre-applied 30 minutes before recording. **(C)** Whole-cell patch-clamp traces in response to pH 5.0 or pH 6.0 + 10 μM T3 under the same pre-treatment and co-application of YM-254890 (n = 5). **, $P < 0.01$; ***, $P < 0.001$.

4. Discussion

In this thesis, electrophysiological methods were employed to investigate the effects of thyroid hormones, particularly triiodothyronine (T3), on acid-sensing ion channels (ASICs), heterologously expressed in *Xenopus laevis* oocytes or HEK293 cells. It was demonstrated that T3 significantly potentiated rASIC1a and rASIC3 currents at micromolar concentrations, though via distinct mechanisms. For rASIC1a, T3 increased the efficacy of protons, whereas for rASIC3, it enhanced proton sensitivity without altering efficacy.

Compared with rat ASICs, human ASICs exhibited a different response profile to T3. While T3 potentiated homomeric hASIC1a currents, it failed to affect hASIC1a/3 heteromers. Notably, T3 directly activated hASIC3 channels under neutral and alkaline pH conditions, and this effect was inhibited by extracellular acidification.

In addition to heterologous expression systems, endogenous ASICs were identified in thyroid gland epithelial cells. Consistent with the response of hASIC1a/3 heteromers, T3 failed to potentiate transient ASIC currents in these cells, suggesting that the endogenous ASICs are likely composed of hASIC1a/3 heteromers.

Interestingly, under conditions of extracellular acidification and T3 application, an outward current was observed in thyroid epithelial cells. Further analysis revealed that this current was carried by K^+ ions and was activated via a GPCR-mediated pathway involving an elevation of the intracellular Ca^{2+} concentration.

4.1. Mechanistic diversity of T3 effects on ASIC channels

4.1.1. Effects of T3 on rat ASICs

In the first part of this thesis, I examined the effects of TH, particularly T3, on rat ASICs. As shown in Figure 6B, all three hormones (T2, T3, and T4) significantly potentiated rASIC1a currents at micromolar concentrations. Given their highly similar molecular structures and comparable ranges of active concentrations, it is likely that they interact with a common binding site on rASIC1a. However, the degree of potentiation differed among the three, despite their shared inner benzene ring structure (Fig 6A). This suggests that the iodine atoms on the outer benzene ring, which vary among T2, T3, and T4, may play a critical role in modulating their efficacy.

A comparable pattern is seen with classical thyroid hormone receptors (TRs). Although T3 and T4 are structurally similar, the binding affinity of T4 to TRs is approximately 20 - 30 times lower than that of T3 [98-100]. This is attributed to the 5′-iodine group on T4, which introduces steric hindrance and interferes with optimal binding to the TR ligand pocket [101]. As a result, T4 is considered a prohormone that must be converted into T3 to become biologically active. In contrast, for integrins, a non-genomic target of TH, T4 often exhibits greater potency than T3 [86].

A similar structural principle may explain the differential effects of thyroid hormones on rASIC1a. Specifically, the position and number of iodine atoms on the outer ring may influence how well the hormone fits into the putative binding pocket on rASIC1a and how efficiently it transduces conformational changes into functional modulation.

The potentiation of rASIC1a and rASIC3 by T3 was reversible (Fig. 7A and Fig. 9A), suggesting that it did not involve covalent bonding. Similar to the interaction of T3 with TRs, T3 may also bind to ASICs through noncovalent forces, such as hydrogen bonding through its carboxyl, amino, or phenolic hydroxyl groups, as well as hydrophobic interactions via the phenol rings. Furthermore, halogen bonding involving iodine atoms on the inner or outer ring may also contribute to ligand-channel interactions [102]. These chemical features may underlie the specificity and potency of T3's modulatory effect on ASICs, but its exact binding pocket remains to be elucidated.

Interestingly, although rASIC1a and rASIC3 belong to the same ion channel family and share approximately 50% sequence identity, the outcome of T3 modulation was different. For rASIC1a, T3 significantly potentiated the peak current amplitude at any pH, thus increasing proton efficacy, and did not significantly shift the proton activation curve (Fig. 8B). By contrast, for rASIC3, T3 enhanced proton sensitivity, as evidenced by a leftward shift in both the activation and steady-state desensitization (SSD) curves (Fig. 11C). Importantly, at pH 6.0, when rASIC3 is fully activated, T3 failed to further potentiate the transient current (Fig. 10A), supporting the notion that T3 does not alter its proton efficacy.

Given their shared sequence homology and the fact that both subtypes are potentiated by T3 in a concentration-dependent manner, it is plausible that T3 interacts with a conserved binding pocket on ASIC1a and ASIC3. However, the different outcome of binding to the two channels could be due to local structural differences surrounding this binding site or intrinsic differences in their gating mechanism.

Although the precise binding pocket of T3 on rASIC channels remains to be identified, several hypotheses can be proposed based on existing functional and structural data. In addition to its effect on window currents, T3 also evoked a sustained current at pH 6.0 in rASIC3, which was absent in the absence of T3 (Fig. 9C). One possible explanation is that T3 potentiated a low pH-induced sustained current of rASIC3. Previous studies have linked this current to the first transmembrane domain (TM1) and the N-terminal region of rASIC3. Supporting this idea, chimeric constructs in which these domains were replaced with the corresponding regions from ASIC1a failed to generate the sustained current [103]. This suggests that TM1 and the N-terminus are critical structural determinants for the sustained current component in rASIC3 and may therefore play a key role in mediating the modulatory effect of T3.

In addition, T3 slowed the desensitization kinetics of rASIC3, as indicated by a larger desensitization time constant (τ) at pH 6.0, even though it did not enhance the peak transient current under these conditions (Fig. 10C). This type of effect is similar to the action of known non-proton ligands such as GMQ, which modulate ASIC3 through a different binding site from the proton-sensing region [58]. These ligands bind to an allosteric site located in the lower palm domain of the channel. In particular, the amino acid residue E79, E423 and its surrounding region have been identified as critical for this form of modulation [104]. The similarity in T3's effect suggests that it may also act through a similar allosteric mechanism.

Taken together, these findings suggest that T3 likely binds to a site on ASICs that is possibly within the palm domain or in regulatory regions such as TM1 or the N-terminal domain. The fact that T3 affected rASIC1a and rASIC3 differently may result from either difference in their gating mechanism or subtle variations in the amino acids surrounding this binding site. These local structural differences might determine whether T3 enhances proton efficacy, as in rASIC1a, or increases proton sensitivity, as seen in rASIC3. To better understand how T3 specifically modulates different ASIC subtypes, future experiments using chimeric channels or targeted mutation of candidate residues will be essential.

4.1.2. Effects of T3 on human ASICs

Compared with rASICs, hASICs responded differently to T3. For homomeric hASIC1a channels, T3 had an effect similar to that observed with rASIC3: it significantly potentiated transient currents at pH 6.5 but not at pH 6.0 (Fig. 14A). This suggests that T3 enhanced the proton sensitivity of hASIC1a without affecting its proton efficacy. These findings also imply that hASIC1a may share a similar T3 binding site with rASICs.

Surprisingly, unlike its potentiating effects on rASIC1a, rASIC3 and hASIC1a, T3 directly activated hASIC3 homomeric channels at neutral pH, leading to a large sustained current. This current increased with increasing T3 concentrations, though with relatively low affinity (EC_{50} > 100 μM). Despite this low affinity, the efficacy of T3 was remarkably high: at 1 μM, the amplitude of the T3-induced current was already comparable to that evoked by pH 5.5, which almost fully activates the channel. In addition, at 20 μM, the T3-induced current was almost 60-fold larger than that elicited by protons. This observation suggests that protons are only a partial ligand at hASIC3 and that T3 is by far more efficient in activating hASIC3 (Fig. 15).

Several other compounds have been reported to activate ASIC3 at neutral pH, including GMQ, neuropeptide RPRFa, and arachidonic acid [57-59]. These agents typically shift the activation and steady-state desensitization (SSD) curves and enhance sustained currents by expanding the pH range at which window currents occur. In contrast, T3 failed to potentiate the transient current of hASIC3 at pH 6.0 (around pH_{50} of hASIC3), implying a mechanistically different mode of action from previously known ligands. This suggests a different binding site than the GMQ binding site in the lower palm domain.

As observed with rat ASICs, T3 was also more effective than T2 or T4 in modulating hASIC3 (Fig. 16A). At equivalent concentrations, T2 induced no detectable current, and T4 elicited only a weak response. This rank order of potency is consistent with their physiological roles, with T3 as the biologically active hormone, T4 as a prohormone, and T2 generally considered inactive in both genomic and non-genomic pathways.

Surprisingly, T3 evoked similar current amplitudes at pH 7.4 and pH 8.0, but the response declined at more acidic pH (e.g., pH 6.5 or pH 6.0; Fig. 16B). Given that the pKa of the phenolic hydroxyl group of T3 is ~8.4 [105], the group is protonated to ~72 % at pH 8.0, to 91 % at pH 7.4, and to > 99 % at pH 6.5 and 6.0. Therefore, the protonation state unlikely accounts for the reduced current at low pH. A more plausible explanation is that acidic pH triggers

conformational changes in hASIC3 that hinder T3 binding or reduce the channel's ability to respond to T3.

Consistent with an ASIC-mediated current, the T3-induced current was also sensitive to amiloride (Fig. 16C). Interestingly, 10 μM amiloride slightly potentiated the T3-induced current, while higher concentrations inhibited it. This biphasic effect has been reported for ASIC3 before, and in those cases, low concentrations of amiloride shift activation/SSD curves to enhance the window current [52].

To assess the ion selectivity of T3-induced currents, reversal potentials were measured for both T3- and proton-induced currents. The reversal potential of T3-induced currents was +36.5 mV, compared with +45.4 mV for proton-induced currents, both consistent with a Na^+-selective conductance (Fig. 16D). The slightly lower reversal potential observed with T3 may reflect a shift in the Na^+ equilibrium potential, possibly due to prolonged Na^+ influx through the sustained activation of hASIC3 by T3.

Notably, with the same amount of RNA injection (~1 μg per oocyte), the proton-induced current amplitude of hASIC3 in *Xenopus* oocytes was relatively small (typically < 0.5 μA), whereas hASIC1 and hASIC1/3 heteromers produced much larger currents (typically > 5 μA) (Fig. 14). A similar observation was observed by Delaunay et al. (2012) [41], where hASIC3 consistently generated smaller currents in *Xenopus* oocytes and mouse cortical neurons, while much larger currents (>1 nA) were recorded in COS cells. This discrepancy suggests that hASIC3 function is highly dependent on the expression system. A plausible explanation is the requirement for specific interacting proteins or membrane-associated factors required for optimal channel assembly, trafficking, or gating, which might be absent in oocytes and mouse neurons, but present in COS cells. Therefore, the hASIC3 currents (including those induced by T3) observed in oocytes may not fully represent the channel's functional properties under physiological conditions or conditions in mammalian cells.

4.2. Response of Nthy-ori-3-1 cells to T3 and acidic pH

4.2.1. Effect of T3 on endogenous ASICs in Nthy-ori-3-1 cells

Because the effective concentrations of T3 observed in ASIC recordings fall within the micromolar range, to better understand how T3 affects ASICs in a setting closer to more physiological conditions, we used the Nthy-ori-3-1 cell line, a model of human thyroid follicular epithelial cells. Using qPCR, we confirmed the expression of both ASIC1 and ASIC3 transcripts in these cells (Fig. 12A). Functional ASIC activity was further supported by the presence of transient pH-dependent inward currents, which were blocked by amiloride, a classical ASIC inhibitor (Fig. 19B). However, the current was neither potentiated by T3 nor accompanied by a large T3-induced sustained current. These findings argue against the presence of hASIC1a or hASIC3 homomeric channels. Furthermore, the desensitization kinetics (τ) of the observed currents more closely resembled those of heteromeric hASIC1a/3 than those of the two homomers (Fig. 13). Taken together, these results suggest that the predominant ASIC subtype expressed in Nthy-ori 3-1 cells is the hASIC1a/3 heteromer.

4.2.2. Outward current induced by T3 and extracellular acidification in Nthy-ori-3-1 cells

Notably, a clear outward sustained current was first observed at pH 6.5 in the presence of 20 µM T3 (Fig. 12C). To further characterize this current, we tested several T3 concentrations and extracellular pH values (Fig. 17A). The results showed that this outward current required both extracellular acidification and T3, suggesting a synergistic interaction of these two stimuli. Strongly acidic conditions (e.g., pH 5.0), elicited the outward current even in the absence of T3 (Fig. 17B). However, with increasing concentrations of T3, the outward current was induced at more moderate acidification, indicating that T3 reduced the pH threshold for activation.

To identify the ionic nature and activation mechanism of this current, we used several ion substitution and pharmacological approaches:

- NMDG-based solution (in which extracellular Na^+ was replaced by $NMDG^+$) demonstrated that the current did not depend on Na^+ (Fig. 19A).
- The current was not blocked by amiloride, confirming it was independent of ASIC-mediated Na^+ entry (Fig. 19B).

- Erev(K) solution (with high extracellular K^+ to shift the K^+ reversal potential to ~-70 mV) abolished the current, indicating it was carried by K^+ ions (Fig. 18).
- Ca^{2+}-free extracellular solution did not abolish the current, but application of ionomycin robustly induced it, suggesting that release of Ca^{2+} from intracellular stores was required (Fig. 19C and 19D).

Consistent with these findings, Ca^{2+} imaging showed that both T3 and extracellular acidification independently triggered intracellular Ca^{2+} elevation (Fig. 20A), with a clear cooperative effect when combined.

Furthermore, the application of YM-254890, an inhibitor of G_q and G_s proteins [96, 97], abolished both the T3/pH-induced Ca^{2+} signal and the outward K^+ current (Fig. 20B). This provides strong evidence that the response was mediated by proton-sensitive GPCR activation, which increased intracellular Ca^{2+} and, in turn, activated Ca^{2+}-dependent K^+ channels.

In agreement, the outward current displayed distinctive kinetics that were characteristic of indirect activation via intracellular Ca^{2+} signaling. Typically, there was a noticeable delay of several seconds between the application of the stimulus and the peak of the current, consistent with a Ca^{2+}-mediated mechanism rather than direct ion channel activation. After reaching its peak, the current gradually declined over time. Interestingly, during the washout phase with normal bath solution, the outward current initially increases transiently before returning to baseline, or even dropping below it (Fig. 17A). A similar kinetic profile has been described for BK channels (large conductance Ca^{2+}-activated K^+ channel) [94], which are classical Ca^{2+}-activated K^+ channels. In those cases, acidification inhibits BK channel activity [106], and removal of the acidic stimulus leads to a transient increase in current as the inhibition is relieved.

4.2.3. Potential Additional Ion Channels in Nthy-ori-3-1 Cells

In addition to ASICs and Ca^{2+}-activated K^+ channels, several lines of evidence suggest the presence of other ion channels in Nthy-ori-3-1 cells. As shown in Fig. 19A and Fig. 19D, replacing the standard bath solution with NMDG or Erev(K) solution resulted in a reduction and enhancement of the baseline (leakage) current, respectively. These observations indicate the presence of both Na^+ and K^+ leak currents at the holding potential of -70 mV.

Moreover, in the presence of YM-254890, which inhibits GPCR signaling, a sustained inward current was observed following the transient ASIC current. A similar inward current also appeared under pH 6.0 stimulation alone, albeit with smaller amplitude (Fig. 20C). The persistence of this inward current in NMDG-based solution in Fig. 19A suggests it was not Na^+-dependent. Instead, it could reflect the activity of Cl^- or Ca^{2+}-permeable channels that are responsive to extracellular acidification.

Additionally, in the presence of YM-254890 and 10 μM T3 at pH 6.0, a marked increase in inward current was detected following the transient ASIC response (Fig. 20C, left). This current had different kinetics than the pH 5.0-induced sustained current (Fig. 20B, right), with a relatively rapid kinetics. These features suggest that the current may be directly triggered by T3 and acidification, independent of both GPCR signaling and intracellular Ca^{2+} response.

4.3. Physiological relevance of the T3 effects discovered in this thesis

In this thesis, I investigated the effects of T3 on ASIC1a and ASIC3 from rats and humans heterologously expressed in *Xenopus* oocytes and HEK293 cells, as well as on endogenous ion channels in the human thyroid epithelial cell line Nthy-ori 3-1. While the effective concentration of T3 required to modulate rASICs was in the micromolar range, much higher than the physiological levels (typically in the nano- to picomolar range), it is noteworthy that T3 was able to induce a small but detectable sustained current in hASIC3-expressing oocytes even at nanomolar concentrations (Fig. 15A). This finding suggests that hASIC3 may have a higher sensitivity to T3 than other ASICs. Moreover, as previously discussed, the observed effect in oocytes may be underestimated due to the absence of essential interacting proteins or cellular components required for full channel responsiveness.

We speculate that in thyroid epithelial cells, local T3 concentrations transiently reach micromolar levels under physiological or pathological conditions. Under acidic conditions and in the presence of T3, we observed a significant increase in intracellular Ca^{2+} levels (Fig. 20A). This Ca^{2+} signal may have important physiological consequences. For instance, elevated intracellular Ca^{2+} is known to activate TMEM16A (ANO1) channels, enhance the activity of dual oxidase (DUOX) enzymes, and promote thyroglobulin iodination–key steps in thyroid hormone synthesis. Moreover, the folding and processing of thyroglobulin is also Ca^{2+}-dependent (Fig. 21).

Additionally, activation of Ca^{2+}-activated K^+ channels by intracellular Ca^{2+} elevation can cause membrane hyperpolarization. This hyperpolarization may facilitate the transport of the electrogenic sodium/iodide symporter (NIS), which co-transports two Na^+ ions and one I^- ion per cycle. A more negative membrane potential would increase the driving force for Na^+ influx, thereby indirectly promoting iodide uptake and supporting efficient thyroid hormone production (Fig. 21).

Together, these findings reveal a potentially multifaceted role for T3 and acidification in modulating ion channel activity in thyroid cells, extending beyond classical genomic pathways and highlighting novel mechanisms of hormone-channel interaction.

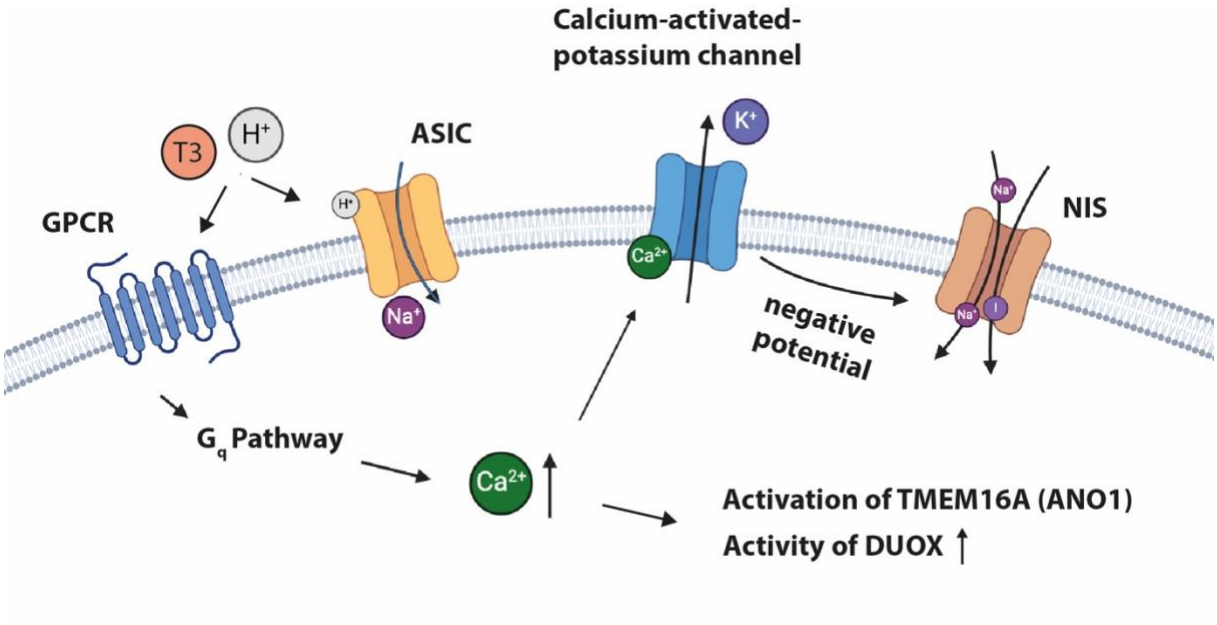

Figure 21. Schematic overview of the proposed mechanism of proton- and T3-induced GPCR and ion channel activation in Nthy-ori-3-1 cells. For details see text.

4.4. Outlook

The findings presented in this thesis uncover a novel, subtype-specific modulation of acid-sensing ion channels (ASICs) by the thyroid hormone T3. Additionally, we also identified a unique mechanism in thyroid gland epithelial cells (Nthy-ori-3-1), in which T3 and extracellular acidification synergistically increase intracellular Ca^{2+}, leading to the activation of a Ca^{2+}-dependent K^+ current. While these results provide new insight into non-genomic actions of T3, several important questions remain to be addressed in future research:

1. What is the precise binding site of T3 on ASICs, particularly across different subtypes?

Although T3 potentiates multiple ASIC subtypes, the underlying mechanisms differ (e.g., enhancing proton efficacy in rASIC1a vs. increasing proton affinity in rASIC3). This suggests that while T3 may bind to a shared or overlapping pocket, the resulting conformational changes are subtype-specific. To determine the exact binding domains and clarify the molecular basis of T3-ASIC interactions, future studies could employ structural modeling with molecular docking, site-directed mutagenesis, or high-resolution techniques such as cryo-electron microscopy (cryo-EM).

2. Why did T3 fail to potentiate the transient current of hASIC3 but instead induced a robust sustained current?

The ability of T3 to activate a sustained current in hASIC3 without affecting the transient current suggests that it may act via a distinct binding pocket or induce a unique gating mechanism. To dissect this mechanism, future studies could perform amino acid sequence alignments between hASIC3 and other ASIC subtypes to identify divergent residues, which could potentially be involved in this different modulation. These candidate residues could then be systematically tested using site-directed mutagenesis to assess their contribution to T3 sensitivity and channel gating behavior. Importantly, the observation that nanomolar concentrations of T3 can directly activate hASIC3 also raises the possibility that T3 might act as a physiological ligand for this channel. This hypothesis could be tested by investigating the ligand-channel interaction using cryo-EM or other structural techniques.

3. Which GPCR mediates the Ca^{2+} response triggered by T3 and acidic pH, and which Ca^{2+}-activated K^+ channel is responsible for the outward current?

Although the GPCR inhibitor YM-254890 abolished both the intracellular Ca^{2+} rise and the outward K^+ current, the specific identity of the GPCR and Ca^{2+}-activated K^+ channel involved remains unresolved. Proton-sensitive GPCRs that signal through the Gq pathway—such as GPR68, GPR4, and GPR132—are likely candidates. Similarly, for the Ca^{2+}-activated K^+ channel, BK (large conductance), IK (intermediate conductance), and SK (small conductance) channels should be prioritized for investigation. To verify these candidates, future studies could employ a combination of transcriptomic approaches (e.g., qPCR), pharmacological profiling using selective inhibitors, and gene knockdown or silencing strategies. These methods will help to elucidate the molecular components of the T3- and acidification-induced signaling pathway in thyroid epithelial cells.

In summary, this thesis provides a new perspective on how the thyroid hormone T3 can directly modulate GPCRs and ion channels, particularly ASICs, beyond its classical genomic actions through nuclear receptors. These findings open a broader view of the non-genomic actions of T3. In the future, a combination of structural, molecular biological, and pharmacological approaches will be necessary to address the unsolved questions raised above, and to fully understand how T3 interacts with ASICs and GPCRs, and what this means for human physiology and disease.

Literature

1. Waldmann, R., et al., *A proton-gated cation channel involved in acid-sensing.* Nature, 1997. **386**(6621): p. 173-7.
2. Qadri, Y.J., A.K. Rooj, and C.M. Fuller, *ENaCs and ASICs as therapeutic targets.* Am J Physiol Cell Physiol, 2012. **302**(7): p. C943-65.
3. Jasti, J., et al., *Structure of acid-sensing ion channel 1 at 1.9 A resolution and low pH.* Nature, 2007. **449**(7160): p. 316-23.
4. Sherwood, T.W., E.N. Frey, and C.C. Askwith, *Structure and activity of the acid-sensing ion channels.* Am J Physiol Cell Physiol, 2012. **303**(7): p. C699-710.
5. Grunder, S. and X. Chen, *Structure, function, and pharmacology of acid-sensing ion channels (ASICs): focus on ASIC1a.* Int J Physiol Pathophysiol Pharmacol, 2010. **2**(2): p. 73-94.
6. Gründer, S. and M. Pusch, *Biophysical properties of acid-sensing ion channels (ASICs).* Neuropharmacology, 2015. **94**: p. 9-18.
7. Yoder, N. and E. Gouaux, *The His-Gly motif of acid-sensing ion channels resides in a reentrant 'loop' implicated in gating and ion selectivity.* Elife, 2020. **9**.
8. Rook, M.L., et al., *beta11-12 linker isomerization governs acid-sensing ion channel desensitization and recovery.* Elife, 2020. **9**.
9. Chen, C.C., et al., *A sensory neuron-specific, proton-gated ion channel.* Proc Natl Acad Sci U S A, 1998. **95**(17): p. 10240-5.
10. Wemmie, J.A., et al., *Acid-sensing ion channel 1 is localized in brain regions with high synaptic density and contributes to fear conditioning.* Journal of Neuroscience, 2003. **23**(13): p. 5496-5502.
11. Wemmie, J.A., et al., *The acid-activated ion channel ASIC contributes to synaptic plasticity, learning, and memory.* Neuron, 2002. **34**(3): p. 463-477.
12. Wemmie, J.A., et al., *Overexpression of acid-sensing ion channel 1a in transgenic mice increases acquired fear-related behavior.* Proceedings of the National Academy of Sciences of the United States of America, 2004. **101**(10): p. 3621-3626.
13. Coryell, M.W., et al., *Restoring Acid-Sensing Ion Channel-1a in the Amygdala of Knock-Out Mice Rescues Fear Memory But Not Unconditioned Fear Responses.* Journal of Neuroscience, 2008. **28**(51): p. 13738-13741.
14. Peng, Z., et al., *ASIC1a affects hypothalamic signaling and regulates the daily rhythm of body temperature in mice.* Commun Biol, 2023. **6**(1): p. 857.

15. Lin, S.H., W.H. Sun, and C.C. Chen, *Genetic exploration of the role of acid-sensing ion channels.* Neuropharmacology, 2015. **94**: p. 99-118.
16. Nakamura, M. and I.S. Jang, *Characterization of proton-induced currents in rat trigeminal mesencephalic nucleus neurons.* Brain Res, 2014. **1583**: p. 12-22.
17. Chang, C.T., et al., *Involvement of Acid-Sensing Ion Channel 1b in the Development of Acid-Induced Chronic Muscle Pain.* Front Neurosci, 2019. **13**: p. 1247.
18. Lee, J.Y.P., et al., *Inhibition of acid-sensing ion channels by diminazene and APETx2 evoke partial and highly variable antihyperalgesia in a rat model of inflammatory pain.* Br J Pharmacol, 2018. **175**(12): p. 2204-2218.
19. Price, M.P., et al., *The mammalian sodium channel BNC1 is required for normal touch sensation.* Nature, 2000. **407**(6807): p. 1007-11.
20. Babini, E., et al., *Alternative splicing and interaction with di- and polyvalent cations control the dynamic range of acid-sensing ion channel 1 (ASIC1).* J Biol Chem, 2002. **277**(44): p. 41597-603.
21. Cristofori-Armstrong, B., E. Budusan, and L.D. Rash, *Mambalgin-3 potentiates human acid-sensing ion channel 1b under mild to moderate acidosis: Implications as an analgesic lead.* Proc Natl Acad Sci U S A, 2021. **118**(8).
22. Sherwood, T.W., et al., *Heteromeric acid-sensing ion channels (ASICs) composed of ASIC2b and ASIC1a display novel channel properties and contribute to acidosis-induced neuronal death.* J Neurosci, 2011. **31**(26): p. 9723-34.
23. Molton, O., O. Bignucolo, and S. Kellenberger, *Identification of the modulatory Ca(2+)-binding sites of acid-sensing ion channel 1a.* Open Biol, 2024. **14**(6): p. 240028.
24. Bässler, E.L., et al., *Molecular and functional characterization of acid-sensing ion channel (ASIC) 1b.* Journal of Biological Chemistry, 2001. **276**(36): p. 33782-33787.
25. Chen, X.M., H. Kalbacher, and S. Gründer, *Interaction of acid-sensing ion channel (ASIC) 1 with the tarantula toxin psalmotoxin 1 is state dependent.* Journal of General Physiology, 2006. **127**(3): p. 267-276.
26. Verkest, C., et al., *Mechanisms of Action of the Peptide Toxins Targeting Human and Rodent Acid-Sensing Ion Channels and Relevance to Their In Vivo Analgesic Effects.* Toxins (Basel), 2022. **14**(10).
27. Diochot, S., et al., *Black mamba venom peptides target acid-sensing ion channels to abolish pain.* Nature, 2012. **490**(7421): p. 552-5.

28. Sun, D., et al., *Structural insights into human acid-sensing ion channel 1a inhibition by snake toxin mambalgin1.* Elife, 2020. **9**.
29. Sherwood, T.W. and C.C. Askwith, *Endogenous arginine-phenylalanine-amide-related peptides alter steady-state desensitization of ASIC1a.* Journal of Biological Chemistry, 2008. **283**(4): p. 1818-1830.
30. Baron, A., R. Waldmann, and M. Lazdunski, *ASIC-like, proton-activated currents in rat hippocampal neurons.* J Physiol, 2002. **539**(Pt 2): p. 485-94.
31. Baconguis, I., et al., *X-ray structure of acid-sensing ion channel 1-snake toxin complex reveals open state of a Na(+)-selective channel.* Cell, 2014. **156**(4): p. 717-29.
32. Wang, X., et al., *Serotonin facilitates peripheral pain sensitivity in a manner that depends on the nonproton ligand sensing domain of ASIC3 channel.* J Neurosci, 2013. **33**(10): p. 4265-79.
33. Lingueglia, E., et al., *A modulatory subunit of acid sensing ion channels in brain and dorsal root ganglion cells.* J Biol Chem, 1997. **272**(47): p. 29778-83.
34. Yan, J., et al., *pH-evoked dural afferent signaling is mediated by ASIC3 and is sensitized by mast cell mediators.* Headache, 2013. **53**(8): p. 1250-61.
35. Su, X., et al., *Interregulation of proton-gated Na(+) channel 3 and cystic fibrosis transmembrane conductance regulator.* J Biol Chem, 2006. **281**(48): p. 36960-8.
36. Chung, W.S., et al., *Extracellular acidosis activates ASIC-like channels in freshly isolated cerebral artery smooth muscle cells.* Am J Physiol Cell Physiol, 2010. **298**(5): p. C1198-208.
37. Jahr, H., et al., *Identification of acid-sensing ion channels in bone.* Biochem Biophys Res Commun, 2005. **337**(1): p. 349-54.
38. Ishibashi, K. and F. Marumo, *Molecular cloning of a DEG/ENaC sodium channel cDNA from human testis.* Biochem Biophys Res Commun, 1998. **245**(2): p. 589-93.
39. Wu, W.L., et al., *Targeting ASIC3 for pain, anxiety, and insulin resistance.* Pharmacol Ther, 2012. **134**(2): p. 127-38.
40. Deval, E., et al., *ASIC3, a sensor of acidic and primary inflammatory pain.* EMBO J, 2008. **27**(22): p. 3047-55.
41. Delaunay, A., et al., *Human ASIC3 channel dynamically adapts its activity to sense the extracellular pH in both acidic and alkaline directions.* Proc Natl Acad Sci U S A, 2012. **109**(32): p. 13124-9.

42. Sutherland, S.P., et al., *Acid-sensing ion channel 3 matches the acid-gated current in cardiac ischemia-sensing neurons.* Proc Natl Acad Sci U S A, 2001. **98**(2): p. 711-6.
43. Yagi, J., et al., *Sustained currents through ASIC3 ion channels at the modest pH changes that occur during myocardial ischemia.* Circulation Research, 2006. **99**(5): p. 501-509.
44. Osmakov, D.I., et al., *Proton-independent activation of acid-sensing ion channel 3 by an alkaloid, lindoldhamine, from Laurus nobilis.* Br J Pharmacol, 2018. **175**(6): p. 924-937.
45. Qin, L., et al., *The Drosophila DEG/ENaC PPK12 is a Na(+) leak channel with a low Na(+) affinity.* Sci Rep, 2025. **15**(1): p. 27457.
46. Ortega-Ramirez, A.M., et al., *A conserved peptide-binding pocket in HyNaC/ASIC ion channels.* Proc Natl Acad Sci U S A, 2024. **121**(41): p. e2409097121.
47. Aguilar-Camacho, J.M., et al., *Functional analysis in a model sea anemone reveals phylogenetic complexity and a role in cnidocyte discharge of DEG/ENaC ion channels.* Commun Biol, 2023. **6**(1): p. 17.
48. Wiemuth, D., et al., *BASIC--a bile acid-sensitive ion channel highly expressed in bile ducts.* FASEB J, 2012. **26**(10): p. 4122-30.
49. Sun, Q. and P. Sever, *Amiloride: A review.* J Renin Angiotensin Aldosterone Syst, 2020. **21**(4): p. 1470320320975893.
50. Leresche, N., et al., *On the action of the anti-absence drug ethosuximide in the rat and cat thalamus.* J Neurosci, 1998. **18**(13): p. 4842-53.
51. Sardet, C., A. Franchi, and J. Pouyssegur, *Molecular cloning, primary structure, and expression of the human growth factor-activatable Na+/H+ antiporter.* Cell, 1989. **56**(2): p. 271-80.
52. Matasic, D.S., et al., *Paradoxical Potentiation of Acid-Sensing Ion Channel 3 (ASIC3) by Amiloride via Multiple Mechanisms and Sites Within the Channel.* Front Physiol, 2021. **12**: p. 750696.
53. Waldmann, R., et al., *Molecular cloning of a non-inactivating proton-gated Na+ channel specific for sensory neurons.* J Biol Chem, 1997. **272**(34): p. 20975-8.
54. Benson, C.J., S.P. Eckert, and E.W. McCleskey, *Acid-evoked currents in cardiac sensory neurons: A possible mediator of myocardial ischemic sensation.* Circ Res, 1999. **84**(8): p. 921-8.

55. de Weille, J.R., et al., *Identification, functional expression and chromosomal localisation of a sustained human proton-gated cation channel.* FEBS Lett, 1998. **433**(3): p. 257-60.
56. Besson, T., E. Linguegliа, and M. Salinas, *Pharmacological modulation of Acid-Sensing Ion Channels 1a and 3 by amiloride and 2-guanidine-4-methylquinazoline (GMQ).* Neuropharmacology, 2017. **125**: p. 429-440.
57. Reimers, C., et al., *Identification of a cono-RFamide from the venom of Conus textile that targets ASIC3 and enhances muscle pain.* Proc Natl Acad Sci U S A, 2017. **114**(17): p. E3507-E3515.
58. Alijevic, O. and S. Kellenberger, *Subtype-specific modulation of acid-sensing ion channel (ASIC) function by 2-guanidine-4-methylquinazoline.* J Biol Chem, 2012. **287**(43): p. 36059-70.
59. Marra, S., et al., *Non-acidic activation of pain-related Acid-Sensing Ion Channel 3 by lipids.* EMBO J, 2016. **35**(4): p. 414-28.
60. Ananchenko, A. and M. Musgaard, *Multiscale molecular dynamics simulations predict arachidonic acid binding sites in human ASIC1a and ASIC3 transmembrane domains.* J Gen Physiol, 2023. **155**(3).
61. Hawashin, A., et al., *Modulation of Acid-Sensing Ion Channels by Tannic Acid and Green Tea via a Membrane-Mediated Mechanism.* ACS Chem Neurosci, 2023. **14**(14): p. 2487-2498.
62. Boron, W.F. and E.L. Boulpaep, *Medical physiology*. Third edition. ed. 2017, Philadelphia, PA: Elsevier. xii, 1297 pages.
63. Chemburkar, S.R., K.C. Deming, and R.E. Reddy, *Chemistry of thyroxine: an historical perspective and recent progress on its synthesis.* Tetrahedron, 2010. **66**(11): p. 1955-1962.
64. Sorimachi, K., *Induction of High Phenolic Pk of Iodothyronines by Sodium Dodecyl-Sulfate - Adaptation to Quantitative-Analysis of the Iodoamino Acid Content of Thyroglobulin.* Biochimica Et Biophysica Acta, 1980. **621**(1): p. 53-62.
65. Marino, M. and R.T. McCluskey, *Role of thyroglobulin endocytic pathways in the control of thyroid hormone release.* Am J Physiol Cell Physiol, 2000. **279**(5): p. C1295-306.
66. Luster, M., et al., *The Thyroid and Its Diseases : A Comprehensive Guide for the Clinician*. 1st 2019. ed. 2019, Cham: Springer International Publishing : Imprint: Springer.

67. Friesema, E.C., et al., *Identification of monocarboxylate transporter 8 as a specific thyroid hormone transporter.* J Biol Chem, 2003. **278**(41): p. 40128-35.
68. Friesema, E.C., et al., *Effective cellular uptake and efflux of thyroid hormone by human monocarboxylate transporter 10.* Mol Endocrinol, 2008. **22**(6): p. 1357-69.
69. Bagga, A.D., B.P. Johnson, and Q. Zhang, *Spatially dependent tissue distribution of thyroid hormones by plasma thyroid hormone binding proteins.* Pflugers Arch, 2025. **477**(3): p. 453-478.
70. Mendel, C.M., et al., *Thyroxine transport and distribution in Nagase analbuminemic rats.* J Clin Invest, 1989. **83**(1): p. 143-8.
71. Boron, W.F. and E.L. Boulpaep, *Medical physiology : a cellular and molecular approach*. 1st ed. 2003, Philadelphia, PA: W.B. Saunders. xiii, 1319 p.
72. Corvilain, B., et al., *Role of the cyclic adenosine 3',5'-monophosphate and the phosphatidylinositol-Ca2+ cascades in mediating the effects of thyrotropin and iodide on hormone synthesis and secretion in human thyroid slices.* J Clin Endocrinol Metab, 1994. **79**(1): p. 152-9.
73. Ohno, M., et al., *The paired-domain transcription factor Pax8 binds to the upstream enhancer of the rat sodium/iodide symporter gene and participates in both thyroid-specific and cyclic-AMP-dependent transcription.* Mol Cell Biol, 1999. **19**(3): p. 2051-60.
74. Kogai, T., et al., *Regulation by thyroid-stimulating hormone of sodium/iodide symporter gene expression and protein levels in FRTL-5 cells.* Endocrinology, 1997. **138**(6): p. 2227-32.
75. Kogai, T., K. Taki, and G.A. Brent, *Enhancement of sodium/iodide symporter expression in thyroid and breast cancer.* Endocr Relat Cancer, 2006. **13**(3): p. 797-826.
76. Jing, L. and Q. Zhang, *Intrathyroidal feedforward and feedback network regulating thyroid hormone synthesis and secretion.* Front Endocrinol (Lausanne), 2022. **13**: p. 992883.
77. Pesce, L., et al., *TSH regulates pendrin membrane abundance and enhances iodide efflux in thyroid cells.* Endocrinology, 2012. **153**(1): p. 512-21.
78. Jang, D., et al., *TSH stimulation of human thyroglobulin and thyroid peroxidase gene transcription is partially dependent on internalization.* Cell Signal, 2022. **90**: p. 110212.

79. Bjorkman, U. and R. Ekholm, *Accelerated exocytosis and H2O2 generation in isolated thyroid follicles enhance protein iodination.* Endocrinology, 1988. **122**(2): p. 488-94.
80. Asghar, M.Y., T. Lassila, and K. Törnquist, *Calcium Signaling in the Thyroid: Friend and Foe.* Cancers, 2021. **13**(9).
81. Corda, D., et al., *Association of the changes in cytosolic Ca2+ and iodide efflux induced by thyrotropin and by the stimulation of alpha 1-adrenergic receptors in cultured rat thyroid cells.* J Biol Chem, 1985. **260**(16): p. 9230-6.
82. Marcocci, C., et al., *Norepinephrine and thyrotropin stimulation of iodide efflux in FRTL-5 thyroid cells involves metabolites of arachidonic acid and is associated with the iodination of thyroglobulin.* Endocrinology, 1987. **120**(3): p. 1127-33.
83. Twyffels, L., et al., *Anoctamin-1/TMEM16A is the major apical iodide channel of the thyrocyte.* Am J Physiol Cell Physiol, 2014. **307**(12): p. C1102-12.
84. Hercbergs, A., *Clinical Implications and Impact of Discovery of the Thyroid Hormone Receptor on Integrin alphavbeta3-A Review.* Front Endocrinol (Lausanne), 2019. **10**: p. 565.
85. Bergh, J.J., et al., *Integrin alphaVbeta3 contains a cell surface receptor site for thyroid hormone that is linked to activation of mitogen-activated protein kinase and induction of angiogenesis.* Endocrinology, 2005. **146**(7): p. 2864-71.
86. Lin, H.Y., et al., *L-Thyroxine vs. 3,5,3'-triiodo-L-thyronine and cell proliferation: activation of mitogen-activated protein kinase and phosphatidylinositol 3-kinase.* Am J Physiol Cell Physiol, 2009. **296**(5): p. C980-91.
87. Wang, Y.G., et al., *Acute exposure to thyroid hormone increases Na+ current and intracellular Ca2+ in cat atrial myocytes.* J Physiol, 2003. **546**(Pt 2): p. 491-9.
88. Sakaguchi, Y., G. Cui, and L. Sen, *Acute effects of thyroid hormone on inward rectifier potassium channel currents in guinea pig ventricular myocytes.* Endocrinology, 1996. **137**(11): p. 4744-51.
89. Chapell, R., et al., *Direct channel-gating and modulatory effects of triiodothyronine on recombinant GABA(A) receptors.* Eur J Pharmacol, 1998. **349**(1): p. 115-21.
90. Moffett, S.X., et al., *L-3,3',5-triiodothyronine and pregnenolone sulfate inhibit Torpedo nicotinic acetylcholine receptors.* PLoS One, 2019. **14**(10): p. e0223272.
91. Deng, H., H. Hu, and Y. Fang, *Multiple tyrosine metabolites are GPR35 agonists.* Sci Rep, 2012. **2**: p. 373.

92. Hart, M.E., et al., *Trace amine-associated receptor agonists: synthesis and evaluation of thyronamines and related analogues.* J Med Chem, 2006. **49**(3): p. 1101-12.
93. Neher, E. and B. Sakmann, *Single-channel currents recorded from membrane of denervated frog muscle fibres.* Nature, 1976. **260**(5554): p. 799-802.
94. Pissas, K.P., S. Grunder, and Y. Tian, *Functional expression of the proton sensors ASIC1a, TMEM206, and OGR1 together with BK(Ca) channels is associated with cell volume changes and cell death under strongly acidic conditions in DAOY medulloblastoma cells.* Pflugers Arch, 2024. **476**(6): p. 923-937.
95. Chen, X. and S. Grunder, *Permeating protons contribute to tachyphylaxis of the acid-sensing ion channel (ASIC) 1a.* J Physiol, 2007. **579**(Pt 3): p. 657-70.
96. Kawasaki, T., et al., *[Pharmacological properties of a specific Gq/11 inhibitor, YM-254890].* Nihon Yakurigaku Zasshi, 2006. **128**(1): p. 23-31.
97. Peng, Q., et al., *Functional evidence for biased inhibition of G protein signaling by YM-254890 in human coronary artery endothelial cells.* Eur J Pharmacol, 2021. **891**: p. 173706.
98. Wejaphikul, K., et al., *Insight Into Molecular Determinants of T3 vs T4 Recognition From Mutations in Thyroid Hormone Receptor alpha and beta.* J Clin Endocrinol Metab, 2019. **104**(8): p. 3491-3500.
99. Ichikawa, K., et al., *Nuclear thyroid hormone receptors in cultured human fibroblasts: improved method of isolation, partial characterization, and interaction with chromatin.* Metabolism, 1986. **35**(9): p. 861-8.
100. Samuels, H.H., F. Stanley, and J. Casanova, *Relationship of receptor affinity to the modulation of thyroid hormone nuclear receptor levels and growth hormone synthesis by L-triiodothyronine and iodothyronine analogues in cultured GH1 cells.* J Clin Invest, 1979. **63**(6): p. 1229-40.
101. Sandler, B., et al., *Thyroxine-thyroid hormone receptor interactions.* J Biol Chem, 2004. **279**(53): p. 55801-8.
102. Bleicher, L., et al., *Structural basis of GC-1 selectivity for thyroid hormone receptor isoforms.* Bmc Structural Biology, 2008. **8**.
103. Salinas, M., M. Lazdunski, and E. Lingueglia, *Structural elements for the generation of sustained currents by the acid pain sensor ASIC3.* J Biol Chem, 2009. **284**(46): p. 31851-9.
104. Yu, Y., et al., *A nonproton ligand sensor in the acid-sensing ion channel.* Neuron, 2010. **68**(1): p. 61-72.

105. Sorimachi, K., *Induction of high phenolic pK or iodothyronines by sodium dodecyl sulfate. Adaptation to quantitative analysis of the iodoamino acid content of thyroglobulin.* Biochim Biophys Acta, 1980. **621**(1): p. 53-62.
106. Zhou, Y., X.M. Xia, and C.J. Lingle, *BK channel inhibition by strong extracellular acidification.* Elife, 2018. **7**.